Current Challenges and Potential Directions Towards Precision Microscale Additive Manufacturing – Part II: Laser-Based Curing, Heating, and Trapping Processes

Article *in* Precision Engineering · December 2020

DOI: 10.1016/j.precisioneng.2020.12.012

CITATIONS
2

READS
97

12 authors, including:

Dipankar Behera
University of Texas at Austin
12 PUBLICATIONS **39** CITATIONS
SEE PROFILE

Samira Chizari
University of California, Los Angeles
23 PUBLICATIONS **104** CITATIONS
SEE PROFILE

Ryan Hensleigh
University of California, Los Angeles
15 PUBLICATIONS **527** CITATIONS
SEE PROFILE

Zhenpeng Xu
University of California, Los Angeles
5 PUBLICATIONS **123** CITATIONS
SEE PROFILE

Precision Engineering 68 (2021) 301–318

Contents lists available at ScienceDirect

Precision Engineering

journal homepage: http://www.elsevier.com/locate/precision

Current challenges and potential directions towards precision microscale additive manufacturing – Part II: Laser-based curing, heating, and trapping processes

Dipankar Behera [a], Samira Chizari [b], Lucas A. Shaw [b], Michael Porter [b], Ryan Hensleigh [c,d], Zhenpeng Xu [c,d], Nilabh K. Roy [a], Liam G. Connolly [a], Xiaoyu (Rayne) Zheng [c,d], Sourabh Saha [e], Jonathan B. Hopkins [b], Michael A. Cullinan [a,*]

[a] Nanoscale Design and Manufacturing Laboratory, J. Mike Walker Department of Mechanical Engineering, The University of Texas at Austin, Austin, TX, USA
[b] Flexible Research Group, Mechanical and Aerospace Engineering, University of California, Los Angeles, CA, USA
[c] Additive Manufacturing and Metamaterials Laboratory, Department of Mechanical Engineering, Virginia Polytechnic Institute and State University, Blacksburg, VA, USA
[d] Additive Manufacturing and Metamaterials Laboratory, University of California, Los Angeles, CA, USA
[e] The George W. Woodruff School of Mechanical Engineering, Georgia Institute of Technology, Atlanta, GA, USA

ARTICLE INFO

Keywords:
Precision machine design
Microscale additive manufacturing
Laser-based processes

ABSTRACT

This article is the second in a four-part series of articles providing an overview of the challenges and opportunities in microscale additive manufacturing (AM) processes with applications in fabrication of high precision micro/nano-products. Laser-based microscale additive manufacturing processes are discussed this article. Compared to the other AM processes, laser-based processes provide several unique advantages, especially in terms of a wide variety of processable materials and high volumetric throughputs. The processes discussed in this paper can fabricate complex microscale features with minimum resolutions ranging from hundreds of nanometers to hundreds of microns. However, there are several fundamental limits and trade-offs which hinder the scalability of these processes. The paper discusses the limits to the materials, resolution, geometry, and volumetric throughput and proposes approaches to mitigate these limits and improve the scalability of laser-based microscale AM processes.

1. Introduction

In part II of this series of articles, laser-based additive manufacturing (AM) processes are explored. Much of the motivation to develop microscale AM processes which use lasers as the energy source for material consolidation comes from the maturity of similar processes in the macroscale. Powder-bed fusion type AM processes like Selective Laser Sintering/Melting and vat-photopolymerization processes like Stereolithography have been widely adopted in several industries. The primary basis for arranging the following microscale processes together is the range of physical mechanisms that come into play due laser-material interaction. This happens because of the wide spectrum of optical and thermodynamic parameters that represent the lasers and the materials used in these processes. From an AM perspective, these processes are divided into two main categories namely laser curing and laser heating. Key optical parameters that need to be determined *a priori* for these processes are monochromaticity, coherence, polarization, spectral density, pulse characteristics, beam profiles, and power characteristics among others. Additionally, material properties defining absorption, heat and mass transfer characteristics, and rheology (not an exhaustive list) are also critical in determining the final part characteristics.

This article discusses five major types of laser-based AM processes that have been used by researchers for fabricating microscale parts. The laser curing/photopolymerization processes are Micro-Stereolithography (μ-SLA), Holographic Optical Tweezing (HOT) and Two-Photon Lithography (TPL). The laser heating processes that are discussed here are Laser-Induced Forward Transfer (LIFT) and Microscale Selective Laser Sintering (μ-SLS). The current state-of-the-art in these processes has been discussed in their respective sections and the fundamental challenges associated with them. The processes have been

* Corresponding author.
E-mail address: michael.cullinan@austin.utexas.edu (M.A. Cullinan).

https://doi.org/10.1016/j.precisioneng.2020.12.012
Received 21 April 2020; Received in revised form 11 December 2020; Accepted 13 December 2020
Available online 31 December 2020

evaluated using the following factors – range of processable materials, feature-size resolution, ability to fabricate true-3D structures and the volumetric throughput. Although all the processes use laser as a source of energy, the process principles for laser-material interaction are vastly different from each other and have been discussed in detail in the following sections. The structure of this paper is similar to Parts I and III [1,2], where the processes and their limitations have been presented, followed by a critical discussion of the possible solutions to these issues.

2. Micro-stereolithography (μ-SLA)

2.1. Description of the μ-SLA process

Stereolithography (SLA) is a popular commercial additive manufacturing technique that uses light and a liquid photo-reactive polymer precursor (i.e. resin) to fabricate 3D parts. In SLA light exposure induces solidification of the resin, and by incorporating a dye, light penetrating into the resin is controlled to the micron range. Through exposing resin with a light pattern, it is possible to build a layer of controlled thickness and structure. Stereolithography typically uses a laser beam to rasterize and solidify liquid monomer. While typical feature sizes for SLA are in the range of 100 μm and above [3,4], employing digital mask and reduction lens, analogous to mask photolithography for patterning photoresist [5], modern micro-stereolithography (μ-SLA) pushes the resolution limits down the sub-100 μm range with precision optics. The technique has an ultimate resolution around 1 μm, but commercially available μ-SLA systems typically have feature resolution from 50 to 100 μm or larger. Many systems incorporate a dynamic photomask or spatial light modulator, whereby a liquid crystal-on-silicon (LCOS) display or dynamic micro-mirror array (DMD) manipulate incident light to form a 2D image [6]. This 2D image forms an entire layer in one exposure; otherwise, scanning spot methods are used. There are two types of systems, top-down (Fig. 1a) and bottom-up, based on the light exposure direction. In the bottom-up system, the light source projects from beneath a liquid resin vat, with a transparent membrane bottom. Resin is sandwiched between the transparent membrane and a build-platform. The light-exposed areas solidify and stick to the build platform. Oxygen diffusion through the membrane may inhibit resin adhesion, or the membrane's inherent inertness prevents solidified resin adhesion [7]. The build platform elevates to replenish resin and repeat the cycle. Top-down systems typically do not have membranes and rely on the liquid resin to self-level before exposure. Stereolithography systems originally relied on lasers light-sources, but many modern systems use inexpensive and robust light-emitting diodes (LEDs), simplifying optics considerably [6]. The ability of μ-SLA to form complex parts as shown in Fig. 1b and c with micron resolution, with relatively simple optics, has made it an immensely popular tool.

2.2. Materials

2.2.1. Materials capabilities and challenges in μ-SLA

μ-SLA has been traditionally limited to stiff acrylic polymers, but recent years have seen significant development of new materials. SLA of urethane acrylates and silicone acrylates have been demonstrated producing materilas with an ultra-high strain of over 1000%, a Young's

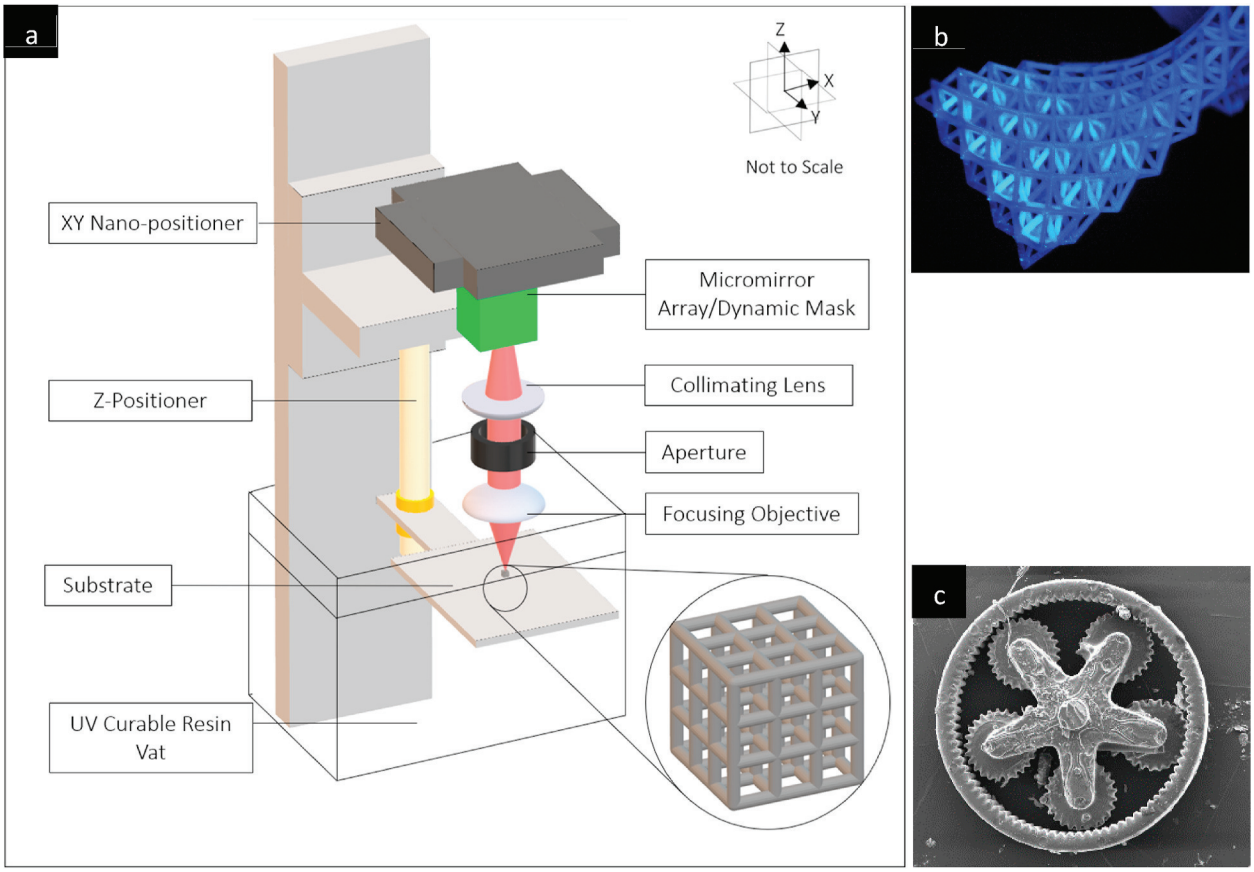

Fig. 1. (a) Simplified schematic of the Microstereolithography μ-SLA process. The z-positioner with the substrate is precisely lowered into the UV curable vat. Light is used to cure the vat in the regions critical for the layer formation using a micromirror array or dynamic mask. The positioner is lowered further to cure the next layer and the process is continued until the final part is fabricated. The excess ink is then removed using a solvent. (b) Optical microscope image of two-phase 3D microlattice using multi-material μ-SLA process [8] (Reproduced with permission from Ref. [8]. Copyright Nature Publishing Group). (c) Scanning electron micrographs for the planet gear set made of polymer-derived ceramic [9] (Reproduced with permission from Ref. [9]. Copyright Materials Research Society 2018).

modulus around 500 KPa, and Sylgard 184-like properties [3,4]. Combinations of low-stiffness and high-stiffness polymers can also create mixtures which span orders of magnitude in stiffness, and have been used to create structures with a large, negative Poisson's ratio via μ-SLA [8]. High-performance polymers including epoxy-acrylate composites [10] and polyimides (Kapton) which can reach 2 GPa Young's modulus and 600 °C thermal stability have also been explored [11]. Further, shape-memory polymers have been demonstrated to create thermally and solvent actuated structures with μ-SLA [12–14]. Pre-ceramic polymers in tandem with thermal pyrolysis have made micro-ceramics of arbitrary complexity readily achievable as well [9,15]. These ceramic microlattices can achieve ultra-high stiffness (100 GPa range) and survive extreme (1000 °C) environments. One can also incorporate inorganic nanoparticles, such as silica, and pyrolyze the initially fabricated structure to fully dense ceramic and glass parts [16]. Controlling the amount of particles in the resin allows for control of structure porosity. Hensleigh et al. combined crosslinked graphene oxide with solvent and a small amount of acrylic monomer to fabricate porous graphene aerogel micro-structures which can serve as catalyst supports [17]. These studies highlight the impressive advancement of μ-SLA materials in recent years from simple acrylic resins to ultra-flexible, medical-grade siloxane, high-performance polymers, and ceramics.

Using μ-SLA combined with nanoscale deposition and post processing, a variety of hollow-tube metallic and ceramic structures have been demonstrated with feature sizes down to tens of nanometers. These methods, however, rely on printing of a microlattice scaffold followed by depositions of thin film materials (metal, ceramic, etc) and etching away of the sacrificial polymer scaffold with chemical or thermal treatment [18–20]. Currently, there is no method to print fully dense metallic structures via μ-SLA, and few methods for functional materials. μ-SLA's high-resolution makes it an intriguing candidate for sensors and implantable devices if the functional material limitation can be overcome. Functional materials typically require high-purity or loading, but μ-SLA's requirement of photo-curable polymers and liquid-like viscosities, limits the loading of functional material, and ultimately the functional (magnetic, thermal, electrical, etc.) performance. Current methods rely on incorporation of metal salts or nanomaterials to create functional objects. Metal salts can be reduced *in-situ* to form conductive nanoparticle composites [21]. Incorporation of piezoelectric nanoparticles allowed Cui et al. to create smart sensors which can sense impact location/direction [22]. However, extensive work to optimize powder suspension stability, resin viscosity, and light penetration depth make processing of functional materials, particular powders, difficult with μ-SLA. Increasing nanoparticle concentration inevitably increases viscosity, which requires one either to limit particle loading, thus degrading material properties, in order to keep viscosity within a useable range. Alternatively, μ-SLA could be modified to handle pastes which is theoretically possible but difficult to achieve in practice without a large detriment to feature resolution.

2.2.2. Possible approaches to overcome materials challenges for μ-SLA

Cui et al. and Yao et al. showed that through careful optimization through surface treatments, processing, and computational modelling, very high-loading of functional materials can be processed to form high-performing and stiff and flexible structures [22,23]. The combination of nanoparticle surface treatment which enhanced performance and particle stability in resin with high-energy ball milling created a μ-SLA ink with very high, loading (30 vol%) but that was also low enough in viscosity for use in membrane based μ-SLA. Higher volume fractions were processable by paste based μ-SLA. Nanoparticle surface functionalization or surfactant addition to compatiblize powder and polymer resins are critical to maintain powder stability in the resin, and reduce viscosity. High-energy ball milling to disperse functional material powder in polymer eliminates agglomerations, and can be scaled to relatively large volumes. Modelling the functional material polymer composite response can guide formulation development, minimize trial-and-error, reducing material development time, and opening new functional materials with unique properties, such as flexibility and high functional performance [23].

There is no clear path forward for printing fully-dense metallic structures via μ-SLA. Metal salt incorporation into the resin, followed by hydrogen gas treatment can produce porous metallic components (~50% porosity), or metals within a polymer matrix, but fully-dense parts have not been realized [21,24]. Optimization of a metal powder resin suspension, similar to Cui et al. [22], in combination with hydrogen gas sintering, could feasibly produce such a structure with extensive sintering to achieve full density, however such a process would require further investigation of resin composition and manufacturing process parameters.

2.3. 3D feature fabrication

2.3.1. Capabilities and challenges in μ-SLA for fabricating 3D features

In principle, there are few limitations to the types of structures that μ-SLA can produce. Fabrication of complex, arbitrary 3D geometries are regularly reported in literature [7,19], however manufacturing limitations do exist. Some extended overhanging features cannot be printed as each layer must adhere to a previous printed feature. For membrane-based systems, there is a suction pressure during recoating, which can destroy slender features, or detach weakly adhered layers [25]. Another difficulty is that the printed part may move or deform during the fabrication process, altering its final shape. This typically occurs when fabricating unbalanced parts or if the solidified resin is unable to sustain the weight of the structure [26]. Part deformation during printing may result in resin curing in incorrect positions, or detaching from the structure altogether. The structure itself may also detach from the build platform entirely if the initial layer bond is not strong enough. Another limitation is the fabrication of closed structures with hollow, internal spaces as resin will remain trapped in the hollow cavity during the post-processing where uncured material is usually removed.

2.3.2. Possible approaches to overcome 3D feature fabrication challenges in μ-SLA

Before printing, careful selection of print design and direction must occur to prevent any free hanging features before beginning manufacturing, since each layer must adhere to a previous printed feature. Overhang structures can be fabricated by adding support to the suspended position. Additionally, the support can be used to balance the printed part so that it is securely tethered to the building platform. Although support solves the aforementioned problems, it will introduce some new challenges. Both designing support and removing support structures require a significant time investment. Support structure will also waste more material than a print without supports. In addition, support may be detrimental to the surface finish after the structure is removed. More efforts must be made to minimize the determinants typically associated with the use of support structures, including increased printing time, cost and impact on surface quality [27].

For printing designs with hollow internal features, one can use bottom-up μ-SLA designs if possible to allow resin to drain during the printing process. Even then, however, resin may remain trapped to some extent. Generally, the design should be modified to incorporate small holes if possible to allow resin cleanout after printing. However, the repair or filling of these holes is difficult, reducing surface quality, and extending overall required production time. The membrane separation force problem is persistent, and there are several possible methods to overcome it. If one can decrease viscosity of the resin, by using a different material or through heat, the effect can be minimized [25]. Some work has also looked at using bioinspired hydrophobic coatings with success, which rely on coating membrane surface with ultra-low adhesive chemicals (fluorosiloxanes) [28]. A general option for higher quality 3D fabrication is to reduce the printing and recoating speed, but

this will increase build time in turn [7].

2.4. Feature size resolution

2.4.1. Feature size resolution capabilities and challenges for μ-SLA

The thickness of each layer as well as the vertical resolution is dependent on the equipment used. Typically, high accuracy positioning stages have a resolution of several microns. Since the light penetration depth is much larger than 10 μm, the only restriction in the layer thickness is the motorized stage's resolution. The lateral resolution of the μ-SLA process can reach several microns. The dynamic pattern generator and the imaging optics determine the achievable minimum feature size in the X–Y plane. Typical dynamic masks used in μ-SLA come in standard resolutions (e.g., 800x600, 1024x768, and 1920x1080) with a standard pixel pitch. The pixel pitch represents the size of each pixel and the space between pixels, and is around 5 μm. Additionally, image non-uniformity from the dynamic digital mask may contribute to non-uniform photopolymerization, compromising feature fidelity and material uniformity. To solve this, Zheng et al., developed a background image correction procedure that subtracts background non-uniformity from the digital mask for each layer [29].

2.4.2. Possible approaches to overcome current limits in feature size resolution for μ-SLA

Many chemistry-based approaches are explored to increase resolution. The spatial area of radicals must be carefully controlled to achieve high resolution. In commercial systems, ambient oxygen acts as a radical inhibitor to minimize their spread through the resin. This is adequate for 10 μm and larger resolutions. However, to successfully enhance resolution through chemical means, one must focus on minimizing, or even actively reducing, the radical population. Scott et al. made use of a unique molecule which can be stimulated by light to form radicals, but these radical are too weak to propagate polymer growth [30]. The group was able to quench or inhibit other polymer propagating radicals with this radical generation mechanism. This, in effect, results in a light-patternable radical inhibitor, or in other words a photo-inhibitor. Using two-wavelengths, one to independently trigger polymerization initiation, the other to inhibit, photopolymerization catalyzation can be contained to a sub-wavelength point well beyond the diffraction limit of the working wavelength of each laser respectively. Scott et al. ultimately achieve a nanometer-scale resolution. A significant drawback is the limited number of molecules which can act as photoinhibitors, limiting wavelength, initiator, and material selection [31].

2.5. Throughput

2.5.1. Throughput capabilities and challenges for μ-SLA

The recoating speed, exposure time, and inherent tradeoffs between resolution and throughput for serial fabrication are the main limits on throughput of the μ-SLA process [26]. The current throughput budget of μ-SLA, for printing optimized acrylate polymers without post-processing, is determined by the efficiency of the exposure process and speed of recoating mechanism. Currently, exposure time of the μ-SLA system varies from 1s to 8s per layer and recoating process varies from 1s to 3s for different resins. With a high resolution requirement such as 20 μm in lateral direction, based on this lower size, this sets an upper limit of 15 mm, due to the standard size of a dynamic mask, resulting in a rate of 27–135 mm^3/min.

By changing the formulation of the resin, either increasing the initiator or decreasing the light-absorbing dye, exposure time may be lowered, but this comes at a cost of resolution. The recoating time is limited by the polymer-settling time, which in itself is determined by resin characteristics such as surface tension, viscosity, and wetting. With bottom-up methods, resin settling time is eliminated. For projecting from above, the settling time can be significant since only gravity drives recoating [26].

2.5.2. Possible approaches to overcome current throughput limits in μ-SLA

The total time currently required to create a layer and recoat fresh resin is ~10 s. The exposure time can be reduced by increasing the exposure power, lowering exposure time needed to properly cure the resin. The recoating process can also be improved by introducing controlled heating. With an increase in resin temperature, the viscosity will decrease, thus lowering the settling time. With the help of an oxygen-permeable window, researchers have demonstrated that the printing speed can be pushed to rates of hundreds of millimeters per hour by using continuous printing methods. The part size can be on the order of tens of centimeters with feature resolution below 100 μm [7]. For large area fabrication, due to the limited resolution of projection devices and various optical defects which are difficult to avoid, the finished part surface quality is deteriorated in turn. Hybrid methods which integrate scanning and projection are demonstrated, enlarging the working area to 400 × 300 mm, a larger platform area than most previous μ-SLA implementations [20,32]. Increasing the layer thickness will also improve the volumetric throughput, however, the vertical resolution will decrease in proportion.

2.6. Prognoses

The micron-scale resolution and high-throughput make μ-SLA one of the most advanced micro-scale fabrication technologies. Advances in optics and the incorporation of scanning mirror mosaic fabrication, have continued to push the limits of resolution and throughput respectively. Material limitations are the most significant challenge for μ-SLA with photopolymerizable polymers being a strict requirement. Research is methodically overcoming this limitation. Polymer derived ceramics have allowed fully-dense ceramic parts to be manufactured. Careful material development of powder composites allows porous (~50%) ceramic or metallic structures when sintered. Powder composites can reach high-functional performance when optimized, pristine dispersion, and high-loading (20–30 vol%) with high-energy ball milling but fully-dense metals are still not possible to fabricate. With further improvements in optics, projection scanning, and materials, μ-SLA will continue to open new and exciting avenues as one of the premier 3D micro-scale additive manufacturing technologies.

3. Two-Photon Photopolymerization/Lithography

3.1. Description of the two-photon lithography (TPL) process

Two-photon lithography (TPL) is a laser-based direct write technique that enables additive manufacturing of millimeter-scale 3D structures with submicron features. The most common implementation of this process involves serial scanning of a tightly focused laser spot in the interior of a photopolymer resist material to generate submicron volumetric pixels (i.e., "voxels") via light-directed polymerization [33]. TPL uses a nonlinear two-photon absorption process to locally polymerize features smaller than the diffraction-limited focused light spot. Thus, features as small as 150 nm can be routinely fabricated using this process. 3D structures can be generated by serially scanning the focal spot in 3D space as shown schematically in Fig. 2a. After printing, the unpolymerized resist is washed away by dissolving it in an appropriate solvent leaving behind a 3D assembly of polymerized submicron voxels. This unique ability of TPL to generate complex 3D structures with submicron features has been widely leveraged to fabricate functional parts for applications such as mechanical and optical metamaterials, bio-scaffolds, photonics, miniaturized optics, flexible electronics, and micromachines.

The sub-diffraction resolution of TPL is a consequence of its underlying two-photon absorption process [35–37]. Two-photon absorption is fundamentally distinct from the more commonly observed single-photon absorption and is a weak and nonlinear effect. Two-photon absorption occurs when two photons of half the energy are near-simultaneously absorbed for the initiation of a molecular

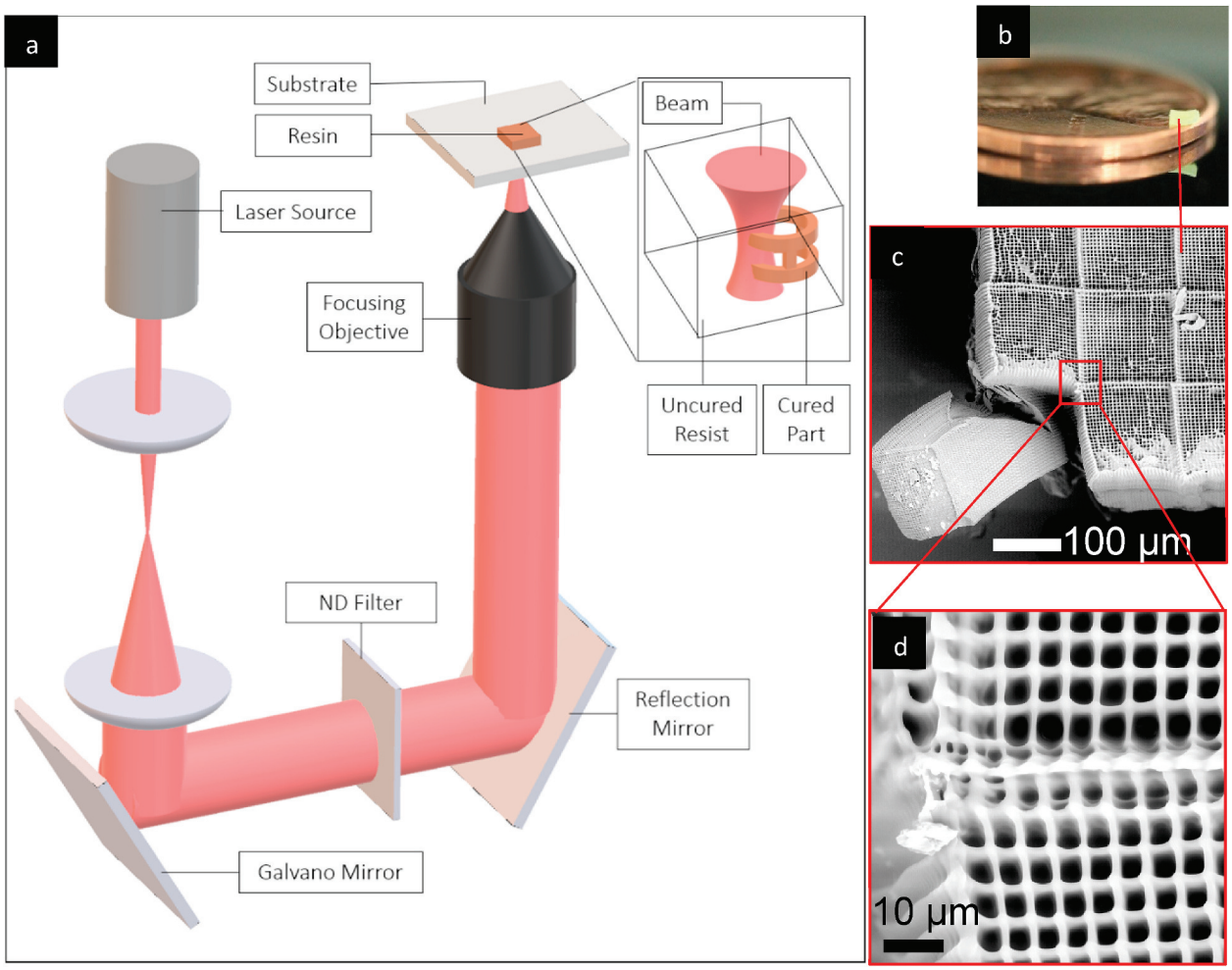

Fig. 2. (a) Schematic of the two-photon lithography process. This process uses laser scanning within a tightly focused spot to polymerize voxels of photopolymerizable resist via the two-photon absorption process. The printed voxel is smaller than the focused light spot. Uncured resist is washed away after printing to leave behind the cured 3D structure. (b)–(d) Optical and scanning electron microscope images of parts fabricated using TPL [34].

transition, instead of a single photon of the full energy. As the probability of simultaneous absorption of two photons is low, high light intensity on the order of TW/cm^2 is required to obtain any appreciable absorption in the photopolymer materials [36]. Therefore, it is possible to spatially restrict two-photon absorption to sub-diffraction volumes by focusing an ultrashort pulsed laser to a diffraction-limited spot. By carefully selecting the laser wavelength and the resist absorptivity, one can ensure that the material polymerizes exclusively via two-photon absorption without any appreciable single-photon absorption. For example, the commonly used UV-curable resists for single-photon polymerization are optically transparent at near-IR wavelengths while being strongly absorbing at half the wavelength. Thus, two-photon polymerization can be performed by selecting a near-IR femtosecond laser and UV-curable resists; this combination has been extensively used in the past to fabricate 3D structures via TPL [38].

3.2. Materials

3.2.1. Materials capabilities and challenges in TPL

TPL is a photopolymerization-based technique that is primarily applied for printing of polymer materials. The most commonly used polymer materials are based on the radical-mediated acrylate chemistry [39] and the thiol-ene chemistry [40,41]. In recent years, biocompatible structures with hybrid inorganic-organic polymers such as OrmoComp have also been printed via TPL [42]. Specific material properties can also be tuned by modifying the polymer backbone on a molecular level, for example, by doping the polymer with iodine [39] or nickel metal [43]. Another common approach to broadening the material pallet involves mixing additives into the resist blend to generate composite structures such as electrically-conductive polymer microstructures loaded with carbon nanotubes (CNTs) [44].

The types of photopolymer materials that can be used in the TPL process are limited by these key functional requirements: (i) optical clarity at the incident wavelength, (ii) high absorptivity at half-wavelength of the incident light, (iii) fast curing chemistries so that localized curing can be performed, and (iv) a match between the refractive index of the resist and the immersion medium of the focusing objective lens so that fine features with minimal optical aberrations can be printed [39]. In combination, these requirements significantly restrict the material design space for TPL as compared to the design space for other photopolymerization techniques that are based on conventional single-photon absorption.

3.2.2. Possible approaches to overcome materials challenges for TPL

The material design space can be expanded by modifying the optical set-up of the TPL system to enable printing of partially-opaque materials; for example, by reducing the length of the light path that passes through the resist material during photopolymerization. Although ad-hoc techniques that modify commercial objective lens to achieve this effect have been demonstrated in the past [45], custom-built

high-numerical aperture objective lenses would significantly accelerate material development for TPL. A careful design of the resist composition to optimize its absorption spectrum versus chemical reactivity can also expand the design space by broadening the writing window. This will enable printing of materials that are unprintable today due to the thermal damage that occurs at high light intensities [46]. Design of photoinitiators for optimal two-photon absorption properties has been demonstrated in the past [47], but follow-up with low-cost and high-throughput organic synthesis schemes is lacking today. An approach that is somewhat underutilized in the field of TPL is printing with pre-cursor materials (such as hybrid polymers) and post-processing the printed structure to convert it into a different class (such as carbon or metals) with widely differing material properties. This approach has been implemented to fabricate carbon [48–50], silicon oxycarbide ceramic [51] and metal 3D structures using TPL. This approach may be explored to expand TPL to ceramics, metals [43], and 3D surface structuring of 2D materials such as graphene. Key challenges for this approach include design of resists with appropriate optical properties, such as optical transparency, and optimization of the process to achieve the desirable functional properties such as electrical conductivity or hardness. Another approach is to modify the stereochemistry, i.e., the three-dimensional molecular arrangement of reacting and non-reacting functional groups, in the components of the resist to speed-up desirable reactions and suppress undesirable side reactions during photo-polymerization. Computational and experimental studies that elucidate the underlying chemical mechanisms of localized photopolymerization would be highly valuable in enabling such a material development approach for TPL.

3.3. 3D feature fabrication

3.3.1. Capabilities and challenges in TPL for fabricating 3D features

The TPL process is particularly well-suited for fabrication of arbitrarily complex 3D structures, including structures that have significant overhangs. For example, Saha et al. have recently demonstrated the ability to print overhanging structures with more than 500 μm long overhangs [34]. The submicron feature size of TPL enables printing of freeform 3D structures whereas its ability to print within the interior of the photopolymer resist enables printing of suspended overhanging sections wherein the unpolymerized resist naturally acts as the support material. The unpolymerized material can act as an effective support material because the density of the polymerized material is similar to that of the unpolymerized material. However, excessive drag forces due to stage motion during printing limit the length of the overhang. True 3D structures can be generated without discretizing the part into 2D layers by using three-axis motion stages to scan the focal spot in 3D space. Limitations to the part geometry are imposed by the optical constraints of the TPL process. These limitations include (i) limited shape of the voxels, (ii) limited height of the parts, and (iii) diffraction-limited resolvability of closely spaced features.

The features in serial-scanning TPL are limited to an ovoid shape due to the nature of the optical intensity distribution in the focal spot of the laser [33]. The aspect ratio, i.e. the ratio of height to width of features, cannot be readily tuned to arbitrary values as the feature size in the axial and lateral directions are linked by the coupling of light intensity distributions in the axial and lateral directions. This limitation on the aspect ratio restricts the discretization of the desired 3D geometry to only those that are feasible with ovoid building blocks. In addition, spherical aberrations often limit the maximum height of the parts to several tens of micrometers. In recent years, the dip-in mode has become popular to overcome this limit [52]; however, it requires one to use only those resists that have a refractive index matched to that of the immersion medium of the lens [39]. Although TPL generates sub-diffraction features on the scale of 150 nm, the ability to print well-resolved fine sub-diffraction features with a spacing of $<$150 nm has not been demonstrated so far. This limitation occurs due to a combination of the optical diffraction limit in resolvability of closely-spaced features and due to the lithographic proximity effect wherein prior printing of nearby features broadens the feature that is currently being printed.

3.3.2. Possible approaches to overcome 3D feature fabrication challenges in TPL

The height of the printed structures can be increased by modifying the optics of the TPL process. Specifically, the dip-in mode can be enabled by using index-matched resists or by modifying the objective lens to minimize spherical aberrations with index-mismatched resists. The voxel shape and the aspect ratio may be tuned by shaping the laser beam or the femtosecond pulse to affect the shape of the optical point spread function during focusing [34]. Similar to a heat affected zone in selective laser melting, sintering, and LCVD process, additional work is required to fully understand the proximity-effect based chemical broadening that limits the resolvability of closely spaced individual features. One approach that has been underutilized so far is to take advantage of the interdependence of the spatio-temporal dynamics of the chemical reactions and the 3D optical intensity distribution to broaden the geometric design space. For example, an optimized resist may be used to suppress writing anywhere except the core of a focused spot even when the focused spot itself may be broad with a distorted intensity distribution due to optical aberrations. Tall structures could be printed with such resists even without satisfying the index-matching criterion. Scientific studies that elucidate these process mechanisms are required to enable this approach.

3.4. Feature size resolution

3.4.1. Feature size resolution capabilities and challenges for TPL

The feature size resolution of TPL is on the order of 120 nm in the lateral direction and it has an axial, i.e., depth resolution two times that of the lateral resolution [53]. More recently, Saha et al. [34] have demonstrated printing of nanowires with axial resolution (i.e., height) less than 175 nm by using a parallel projection technique. Features smaller than this size can be printed in the form of a single 2D layer attached to a substrate by printing only the top sections of the voxels [54]. However, the true 3D resolution is not measurable in such structures; instead, the resolution is quantified by measuring the width and height of suspended nanowire benchmark structures [53]. There are several factors that limit the resolution of TPL. As this is an optically-driven process, the achievable minimum feature size is still limited by the optical point spread function. The factors that limit the resolution of TPL are: (i) the size of the focused light spot that cannot be reduced to an infinitesimally small point due to diffraction limits, (ii) the spatio-temporal growth of the polymerization reaction front, (iii) the thresholding behavior of the resist, and (iv) the mechanical properties of the polymerized features. Resists in which the chemical reaction fronts rapidly proceed outward from the center of the focused spot generate thicker features. Resists in which this effect is suppressed may generate features with lower degrees of conversion that may not exceed the threshold for writing. In addition, even if very thin features could be printed with TPL, these structures may not survive the stresses generated via capillary forces during the post-print development process due to the low strength of the printed structures. In combination, these effects limit the resolution of any specific TPL configuration.

3.4.2. Possible approaches to overcome current limits in feature size resolution for TPL

The classical technique of reducing the size of the diffraction-limited focal spot by reducing the wavelength of light may not be a very successful approach for TPL. Although reducing the wavelength of light does indeed reduce the size of the optical focal spot, it does not guarantee that the printed features will be smaller than those printed with higher wavelength light. This is because the resist may be highly

absorbing in the single-photon mode at lower wavelengths which may lead to over-polymerization. Nevertheless, novel optical techniques that can reduce the optical point spread function without modifying the incident wavelength would have a direct and predictable influence on the resolution of TPL. A different material-based approach to improving the resolution involves optimizing the resist composition by balancing the photo-absorption versus chemical reactivity to generate smaller features via dosage thresholding control. The resolution may be further improved by optimizing the resist and the writing conditions to generate stronger features that can survive the development process. The underlying mechanisms that determine the spatio-temporal growth of the degree of conversion and the strength of the features have not been well-studied in the past. Predictive models that can link writing conditions, resist composition, and optics to the feature size and mechanical properties would play a critical role in identifying practical strategies that can further improve resolution.

3.5. Throughput

3.5.1. Throughput capabilities and challenges for TPL

The volumetric throughput of TPL is limited by its serial point-by-point writing mechanism. The throughput is determined by the linear scanning speed of the focal spot of the laser and the size of the printed voxels. Although slow piezo-scanning stages were used for early work in this field [53,54], contemporary TPL processing is often performed using high-speed galvanometric stages that can scan at linear speeds of ~1 cm/s[52]. For high-resolution writing conditions that generate features smaller than ~300 nm, the volumetric throughput of TPL is ~0.02 mm^3/h [52]. The volumetric throughput can be increased by a factor of ~10 times for low-resolution printing conditions that generate larger voxels. Although it is theoretically possible to increase the volumetric throughput by increasing the scanning speed, the scanning speed cannot be increased to arbitrarily high values due to several practical limitations. These limitations are: (i) at high scanning speeds, the net optical dosage will fall below the threshold values for onset of writing with current laser technology and (ii) at high scanning speeds, the dynamics of the scanning stage during raster scanning in a finite-sized field-of-view limits the overall duration of scan. Holographic techniques have been used in the past to increase throughput by splitting the beam into multiple identical focal spots that can be scanned in parallel either using motion stages or via holographic techniques [55]. Although these techniques parallelize the TPL process, to date, the highest throughput of these techniques has not exceeded the 0.02 mm^3/h throughput achieved by the galvo-based single-point scanning techniques [34]. This is due to a combination of limited pulse energy of the femtosecond lasers that prevents massive parallelization of the process, slow scanning speed of the motion stages, and slow speed of the spatial light modulators (SLM) that are used for generation of the holographs. It is important to note here that although high pulse-energy femtosecond lasers are commercially available in the form of low repetition rate systems, such lasers cannot be used in combination with multi-foci holographic high-speed scanning techniques because scanning with such lasers would lead to intermittent writing due to their low repetition rate (i.e., pulse generation rate).

3.5.2. Possible approaches to overcome current throughput limits in TPL

One approach to increase the throughput of serial techniques is to upgrade the serial systems with galvo-scanning stages than can scan at higher speeds and accelerations. For example, a high-speed writing system was recently demonstrated by Hahn et al. [56]. In conjunction with this modification, one would also need to modify the laser and the resist to support high-speed writing. Specifically, the pulse energy of the laser must be increased so that dosage values above the threshold can be achieved even during low exposure conditions encountered during high-speed writing. In addition, the resist must be modified so that significant dark polymerization reactions can occur. This will ensure that the degree of polymerization exceeds the threshold value even when the duration of exposure is low. Within the context of TPL, it is currently unknown as to how this modification to the resist's thresholding behavior could be achieved.

A different approach to increasing throughput is to massively parallelize the process. Although several techniques have been implemented in the past [55,57], none were able to increase the throughput without comprising the submicron resolution and/or the ability to fabricate arbitrarily complex 3D structures. To massively parallelize TPL, it is highly desirable to implement a layer-by-layer projection scheme that is analogous to the existing projection micro stereolithography techniques for single-photon polymerization [6]. In the past, such projection techniques were unable to achieve any depth resolvability during TPL due to the challenges involved in projecting thin sheets of femtosecond light [57]. To successfully implement depth-resolved projection TPL, one would need to simultaneously optimize the spatial and temporal properties of femtosecond pulses during projection. Saha et al. [34] have recently demonstrated that this is possible through temporal focusing of high-bandwidth femtosecond pulses. Their femtosecond projection parallelization technique (FP-TPL) has now increased the throughput of TPL by up to three orders of magnitude (i.e., volumetric throughput of 10s of mm^3/hr) while maintaining the ability to print thin nanowires of <175 nm width and complex 3D structures. As this is a relatively novel approach to TPL printing, more work is required to improve the predictive capability of the FP-TPL process.

3.6. Prognoses

The unique ability of TPL to generate sub-diffraction nanoscale features in complex 3D geometries is highly valuable in fabrication of a wide variety of functional micro and nanoscale structures such as mechanical and optical metamaterials, bio-scaffolds, photonics, miniaturized optics, flexible electronics, and micromachines. Major barriers to industrial-scale adoption of TPL include low throughput, lack of compatible materials, and lack of process knowledge. Recent advances in parallelization of the process have increased the throughput by up to three orders of magnitude that now make this process competitive with other high-throughput micro AM techniques. Nevertheless, materials challenges and lack of adequate process knowledge still remain as barriers to adoption. Novel printing techniques that bypass the current materials challenges and scientific investigations that advance the understanding of the fundamental process mechanisms of TPL are promising approaches to solve these problems.

4. Laser induced forward transfer (LIFT)

4.1. Description of the LIFT process

Laser Induced Forward Transfer (LIFT) is a maskless and non-contact direct patterning process that uses a high-power pulsed laser to volumetrically deposit material on to the substrate. The process uses a top substrate which is transparent to the laser (tailored to the wavelength used) and has a thin film coating (donor layer) of the material to be deposited. As the laser interacts with the material near the interface of the transparent substrate and the donor layer, local material is ejected on to the bottom substrate, or acceptor. The mechanisms driving ejection manifest at a threshold fluence which varies for different materials, beyond which different ejection regimes are observed. Energy transfer for ejection is generally induced by pressure differentials or thermal stresses [58–60]. Depending on the material and thin film properties, the donor material can be ejected before or after undergoing a phase change. In one regime the solid film can be ejected in the form of 'pellets' formed because of crack propagation and mechanical fracture upon laser-material interaction. Alternatively, localized heating of a solid-liquid film can also generate a cavitation bubble by ablating

material (after phase change for solid films), which expands to form a primary jet [59]. At lower fluences, the jet can recede and inhibit the ejection as the material fills the cavity. Alternatively, at higher fluences, multiple unstable jets and satellites can be formed due to sudden changes in pressure. Optimizing the fluence can produce a stable and continuous jet configuration which will accumulate the liquid into a sessile droplet when the viscocapillary forces and surface tension are overcome [59]. The highest volumetric resolution, or the smallest voxel sizes, are obtained at threshold laser fluences. The jetting and droplet formation characteristics are dependent on the rheological properties (for fluid-driven transfer), mechanical properties (for pellet-drive transfer), laser fluence, film thickness and the gap between the donor and acceptor. Fig. 3 shows the schematic of LIFT and some of the parts that have been fabricated using this process.

The noncontact, maskless, high speed printing characteristics coupled with material independence make LIFT a micro/nano-AM method of significant research interest. LIFT has demonstrated a plethora of applications in flexible electronics, MEMS devices, and biomaterial writing [60,61]. However, the complex physics and narrow processing windows present significant development and scalability challenges for additively manufacturing microparts using LIFT. The following sections outline possible solutions to address them using novel approaches.

4.2. Materials

4.2.1. Materials capabilities and challenges in LIFT

LIFT has been used to deposit a variety of materials such as metals (Cu [63], Ag [64], Au[65], Pt [66], Cr[66], Al [67,68]), semiconducting materials [69] like Ge and Se, oxide layers, nanocomposites [70], conductive polymers (PEDOT-PSS) [71], biomaterials [72] and superconductors [73] among others. Donors with viscosities ranging from 10 to 100000 cP have been printed with LIFT [60,74]. Accurate control of the ejection regimes and use of nanoparticle inks has driven the fabrication of submicron voxels in LIFT. However, donor layer properties, energy transfer mechanism, and phase transformation largely limits the deposition of different materials using LIFT. For example, unstable satellite formation is commonly observed when using low viscosity (<20 cP) nanoparticle inks such as the ones traditionally developed to avoid clogging in nozzle based DW processes and agglomeration. In addition, the direct impingement of the laser on the donor layer can damage the donor due to uneven thermal loading for materials with poor absorption. As such the material compatibility of the LIFT process is also dictated by the type of laser being used.

Fluids which are transparent to the laser cannot be printed using traditional LIFT. Further the structural homogeneity, chemical and biological activity, and electrical properties can be affected due to irreversible phase transformation during melting, and formation of interfacial layers between overlapping deposits. The donor material wettability on the substrate is also critical for fabricating 3D structures. The susceptibility to oxidation of the molten donor layer and rapid quenching may also lead to poor adhesion to the substrate.

4.2.2. Possible approaches to overcome materials challenges for LIFT

The printing of low viscosity inks can be accomplished by partially drying the inks to remove the solvents and obtain a high viscosity/paste-

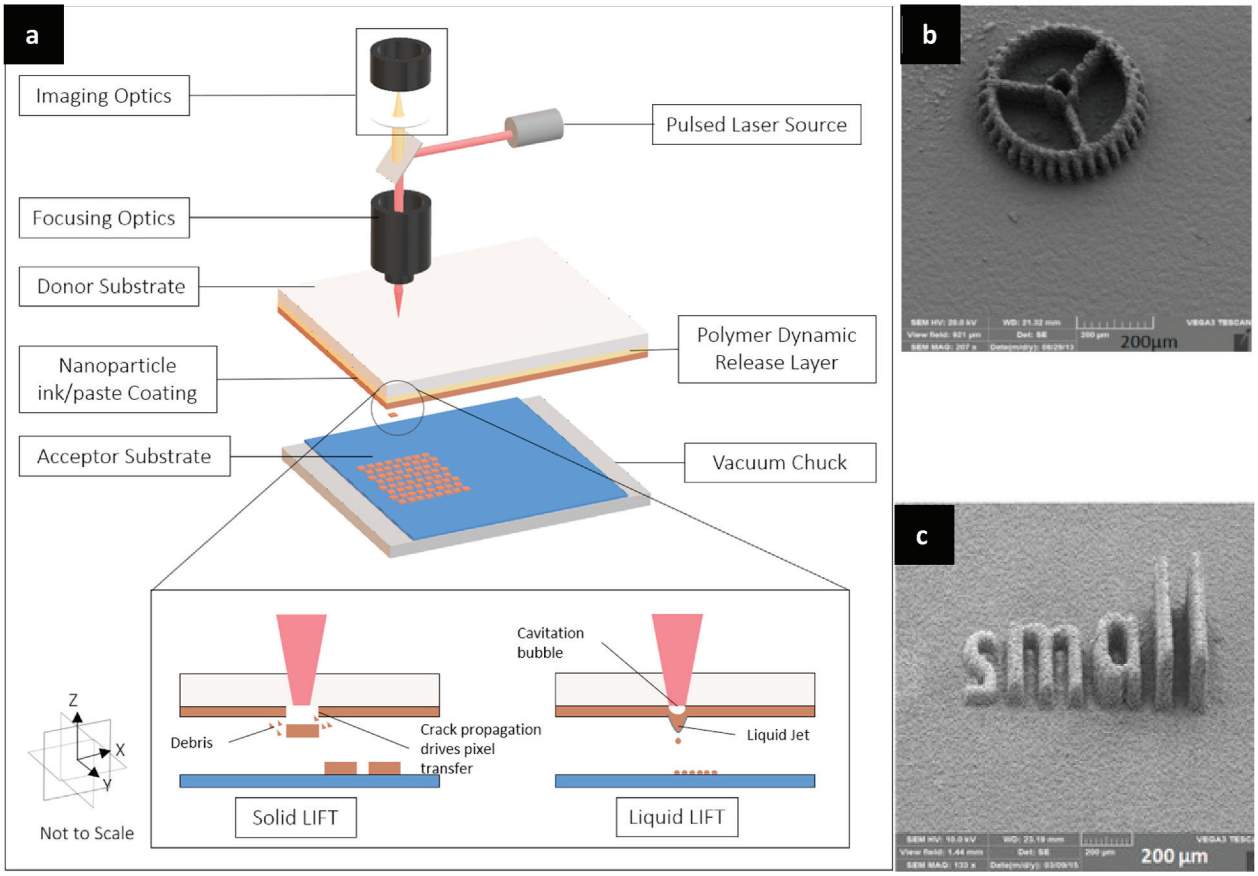

Fig. 3. (a) Schematic diagram laser induced forward transfer (LIFT) process showing the two main modes of pattern transfer (Solid LIFT and Liquid LIFT). When the laser interacts with the material near the interface of the transparent substrate and the donor layer, local material is ejected on to the bottom substrate, or acceptor. The ejection is primarily driven by pressure differentials due to thermal stresses. (b) (scale bar = 200 µm) Scanning electron micrograph of a LIFT printed 'gear' [62] (Reproduced with permission from Optics Express) (c) SEM images of progressing high aspect ratio 2.5D features printed using LIFT (Reproduced with permission from Small – Wiley Online Library).

like ink. These nanopastes transfer on to the substrate as a solid under shear such that the ejected layer is congruent to the spatial profile of the laser. This enables better resolution control and microstructural uniformity by avoiding any melting and condensation. Photolytic or pyrolytic damage to the donor layer due to direct interaction with the laser can be minimized by using an intermediary layer [59,60]. The intermediary layer can be an absorptive material (metal/metal oxide) which is heated by the laser with the donor layer underneath, providing a buffer to ensure uniform localized heating and ejection of the donor. An alternative indirect forward transfer mechanism uses a sacrificial material with a low ablation threshold to avoid contact between incident photons and the donor material. The sacrificial layer triggers the ejection of the donor due to the cavitation pressure created by its vaporization. However, this sacrificial dynamic release layer (DRL) can contaminate the donor with residual particles [66,75]. A variant of this approach uses a thick polymer film with a thickness greater than the laser penetration depth (~2 μm) [76] to absorb the laser and deform into a blister. As the blister grows, it drives flow of the donor layer fluid to the point of ejection and returns to its original shape without contaminating the liquid. These indirect LIFT processes can also enable the deposition of previously incompatible, laser-transparent fluids [59]. However, the effectiveness and uniformity of these multilayer materials is difficult to determine and must be evaluated extensively using time resolved studies and simulations to predict vapor bubble growth.

4.3. 3D feature fabrication

4.3.1. Capabilities and challenges for fabricating 3D features

The voxel-based deposition approach of LIFT has been used to demonstrate fabrication of layer-by-layer in-plane and out-of-plane structures. The ability to fabricate pillar-like structures, overhanging and 3D stacked features including freestanding structures has made LIFT a viable alternative to lithographic processes [61,77]. Single-step multilayer 3D structures, which could include an insulator and a conductor, or an insulating layer between conductive layers, can be fabricated by leveraging different transfer mechanisms. However, there are several challenges associated with seamlessly achieving 3D structures using LIFT. The in-flight mechanics of the donor layer features affect the accuracy of positioning of the individual voxels [78]. Further, error in positioning of individual layers becomes more challenging as the gap between the substrate and the donor layer increases. For solid-LIFT processes, the high ejection velocities can lead to the generation of shock waves which reflect from the substrate and damage the incoming voxels [68,75,79]. For fluid-LIFT processes, high laser fluence (>100 mJ/cm^2) can increase the ejection velocities and lead to the formation of micro- and nano-scale particle debris [75,80,81]. Additionally, the mechanical and thermal strain introduced during the transfer can degrade the overall performance of the structure compared to the bulk donor material. Poor interlayer adhesion can significantly affect the aspect ratio of 3D functional structures in the absence of significant post processing steps. Furthermore, the deposition kinetics, energy transfer and phase change mechanisms produce poor near net shaped parts for high-resolution LIFT (sub-5 μm) with uncontrolled surface roughness. Thus droplet positioning accuracy, interlayer adhesion and high surface roughness are the main limiting factors in production of high-aspect ratio 3D structures using LIFT.

4.3.2. Possible approaches to overcome 3D feature fabrication challenges for LIFT

The inherent limitations of voxel-based layer-by-layer printing of out-of-plane structures can be addressed using sacrificial materials as support structures. The shock wave generation can be minimized by reducing the gap between the donor and the substrate. 3D structure fabrication using LIFT requires a better control over the spatial accuracy of the ejected material. This has been primarily achieved by a variant of LIFT, Laser Decal Transfer (LDT) [82]. Through deposition of high viscosity nanopastes which are identical to the spatial profile of the laser, LDT drives the ejection of the material by shearing the thin film rather than forming a pressure jet. The ejection velocities in LDT are an order of magnitude lower than those in traditional LIFT. However, the transfer distances in LDT must be in the order of hundreds of microns as they can fold and disintegrate during flight, thereby affecting the spatial congruence of the transfer. Printing brittle materials and thicker films (>1 μm) may be difficult for LDT as the mechanical forces required to shear the film would be very high and could lead to unstable printing. A possible approach to this problem is to introduce variable energy profiles at the breakdown regions of the film (edges) and transfer the rest of the pattern under lower fluences. Rapp et al. used this approach to transfer >1 μm thick polymer films. Although using high viscosity nano-suspensions for LDT can reduce ejection velocities [74,82] and improve spatial control of the structure, it does not ensure a good adhesion between the layers. LDT fabricated parts might require subsequent sintering to promote interlayer adhesion. Additionally, these nanopastes must undergo a controlled ageing cycle to produce self-supporting structures.

As found in several studies, ejecting drops at threshold fluences leads to the deposition of spherical or toroidal features [60,61,77,81] which limit the contact area during voxel-by-voxel printing, effectively increasing the porosity of the part. Visser et al. [77] transferred sub-10 μm pure metal droplets by using lasers with a 6.7 ps pulse duration at fluences above threshold to achieve flat disks on the substrates. Compared to the spherical droplets, these disks improved the adhesion between the substrate and the stacked-up layers. High pulsed lasers are critical in transferring the droplets with a high position accuracy, and lower heat-affected zones, avoiding high thermal cycles. Further, intermediate sintering steps can be included to ensure complete material consolidation. The cycling and quenching times can also be increased by depositing the material on heated beds, thereby reducing residual thermal stresses in the structure. However, the residual stresses are ultimately still dependent on the type of material, dynamic release layer and substrate that are employed, and further characterization is needed to improve the fabrication of true-3D layers using LIFT. Post-deposition morphological and microstructural characterization techniques have been integral to LIFT [83,84]. In-situ temporal imaging techniques using pump and probe lasers [85], stroboscopic imaging and high-speed video capture (up to 100,000 fps) [86] have facilitated the understanding of complex phenomena associated with the material transfer process.

4.4. Feature size resolution

4.4.1. Feature size resolution capabilities and challenges

The minimum reported feature size obtained in a 3D structure fabricated using LIFT is ~4 μm[67]. The minimum volumetric resolution that can be obtained typically corresponds to the threshold fluence at which the ejection occurs. Although submicron droplets can be achieved using LIFT, the effective diameter of the deposited feature is enlarged upon impact [67,77]. As discussed in the previous section, stacking up high viscosity, thermally cycled high resolution droplets in a non-controlled environment, can lead to porous structures with poor interlayer adhesion. Therefore, the true resolution of the process is generally higher than the diffraction limited resolution, in order to facilitate robust 3D structure fabrication. The resolution of the process is also affected by the formation of debris on the donor layer due to high fluence or low viscosity inks [60,74]. The resolution of LDT depends on the spatial profile of the beam, as the deposited feature must be congruent to the laser shape and size. Yamada et al. experimentally identified the relationship between the laser spot size and resolution [87,88]. However, there are no replicative studies identifying a similar analytical relationship between the beam profile and true transfer resolution for different LIFT regimes. Predicting the resolution of the process remains a significant challenge for LIFT. Furthermore, printing continuous lines using adjacent deposits and overlapping grid like

structures can lead to material accumulation at the contact points, forming bumps and reducing the effective resolution of the process.

4.4.2. Possible approaches to overcome resolution challenges in LIFT

The material transfer or ejection regime plays an important role in determining the spatial resolution of LIFT. For most material and substrate configurations, the minimum feature size is limited by the diffraction-limited resolution [59,60,74]. In traditional LIFT, the droplet ejection occurs when the cavitation bubble expands from the donor-substrate interface to the free surface, and the fluence is higher than the viscocapillary and surface tension forces. An alternative to this phenomenon is when the laser directly interacts with the free surface of a solid material. This direct interaction melts the material in the irradiated region, locally increases the pressure, and creates a compressive stress in the region [66,89]. To relieve the stress, unloading tensile forces redistribute the molten materials towards the center of the irradiated zone. This creates a jet smaller than the diameter of the beam. Controlled detachment of this jet under optimal laser fluences can lead to the ejection of a high-resolution spherical Au nanodroplets (180–1500 nm) on to the substrate [65,89,90]. However, this backward transfer process is limited by laser transparent substrates and has relatively smaller process windows.

Spatial light modulators have also been used to fabricate single step layer-by-layer parts using LIFT, hence making it easier to produce grid-like patterns. However, their printing resolution might be limited by the maximum diameter of adjacent cavitation bubbles for multiple ejection points and interaction of these bubbles can lead to unwanted perturbations during the material ejection process, therefore degrading the transfer onto the substrate [60,81,91].

4.5. Throughput

4.5.1. Process throughput capabilities and challenges

The maximum reported volumetric throughput of the LIFT process is around 3 x 10^{-6} mm [3]/s with a nominal resolution of 4–6 μm features [77]. Like other laser-based AM processes, digital micromirror arrays (DMDs) and spatial light modulators (SLMs) have been used in LIFT to modulate light in a reconfigurable manner for projecting patterns on the substrate through the donor layer [92,93]. However, the main challenge associated with this parallelized approach is the minimum feature size that can be obtained without degrading adjacent patterns as the cavitation bubbles and shear lengths might overlap and affect the pattern quality [81,91].

4.5.2. Possible approaches to overcome throughput challenges in LIFT

For a production scale adoption of LIFT, further investigation of the process windows must occur to fabricate true-3D parts repeatably. LIFT of nanopastes has been most widely used for producing 3D structures. However, the ageing and drying cycles of the nanopastes must be optimized to print high density parts as well as maximize the throughput [60,86,94]. The limiting features of single DMD LIFT can be overcome by further parallelizing the process, where the overall part density can be improved by using multiple DMDs, without degrading the adjacent patterns. A novel hybrid approach was used by Kuznetsov et al. to combine nanosphere lithography and LIFT to transfer predetermined arrays of nanostructures on the substrate [90,95]. An array of gold nanoparticles was thermally deposited on monodispersed colloidal spheres. A hexagonal array of gold triangular prisms is obtained post removal of the colloidal spheres, creating islands of donor material on the substrate. A laser induced forward transfer of these triangular prisms leads to the coalescence of these prisms into nanodroplets due to high surface tension [95]. The independent control of the size and the periodicities of these arrays makes this hybrid approach a promising variant of LIFT. However, 3D applications have not been demonstrated with this approach yet.

4.6. Prognoses

Laser-induced Forward Transfer (LIFT) has been adopted by several research and industrial organizations to print production-scale organic electronics, gas sensors, biosensors and 2D conductive structures. The 3D fabrication capabilities of LIFT are mainly limited by material adhesion to substrate and adjacent layers, in-situ material consolidation steps, true feature-size resolution, and overall throughput of the process. However, the novel physics of the process can allow for the fabrication of high-resolution non-planar parts independent of the material. Further development is needed to correlate the energy parameters, beam profiles, and pulse times of the lasers with donor and substrate properties to ensure effective material transfer. For layer-by-layer fabrication, accurate positioning of the material is necessary to create good adhesion and functional structures. Spatial light modulators play an important role in 3D structure fabrication using LIFT as they improve the minimum feature-size and speed of the process. Additionally, better resolution and throughput are achieved by using Laser-Induced Backward Transfer (LIBT) and hybrid approaches involving subtractive manufacturing techniques for donor preparation. Additional modeling data for different material transfer regimes would be extremely useful in offsetting the high process experimentation and development costs to make LIFT feasible beyond the laboratory scale.

5. Microscale Selective Laser Sintering (μ-SLS)

5.1. Description of the μ-SLS process

The Selective Laser Sintering process (SLS) is a commercially successful, layer-by-layer additive manufacturing process for rapid prototyping and production-scale fabrication of 3D macroscale parts [96–99] with a wide array of capabilities for the process in aerospace [100], energy [101], and medical implants [102] sectors. However, most commercially available SLS tools are limited to feature size resolutions of greater than 100 μm due to their large laser focal spot size, use of powders with ~100 μm particle sizes, and poor control over thermal and oxidation effects which can result in part porosity and rough surface finishes at the microscale [103,104]. The Microscale Selective Laser Sintering (μ-SLS) process overcomes many of these limitations through the use of precise focusing optics, nanoparticle (NP) inks, and short exposure times and can produce sub-10 μm metallic parts with true-3D structures [105]. As shown in Fig. 4a, in the μ-SLS process, a slot die coating system is used to deposit a layer of nanoparticle ink on to a substrate where it is heated and dried to form a uniform layer of NPs. The substrate is then shuttled to the optical subsystem where a DMD micromirror array is used to project a CW/QCW 808 nm diode laser through a set of focusing objectives and on to the nanoparticle coated substrate, sintering them in the desired pattern. This optical setup has a minimum achievable feature size resolution of ~1 μm and can pattern up to ~2 million spots simultaneously. Once the NPs in the first layer have been sintered, the substrate is brought back to the coating subsystem where a new layer of NPs is deposited on top of the sintered layer and the process repeated until the full 3D part has been built up. Finally, the excess NPs are washed away and the part annealed to improve its electrical and mechanical properties. This process is outlined in Fig. 1a and a more detailed overview of the different subsystems of the μ-SLS development tool can be found in Ref. [106]. Fig. 4b and c shows some of single layer microparts that have been fabricated using the μ-SLS tool.

5.2. Materials

5.2.1. Materials capabilities and challenges in μ-SLS

Most commercially available thermal sintering tools are limited in feature size resolution due to the large particle sizes in the powder used, which are typically in the hundreds of micron range [106,107]. To fabricate microscale parts with sub-10 μm features, finer powders in the

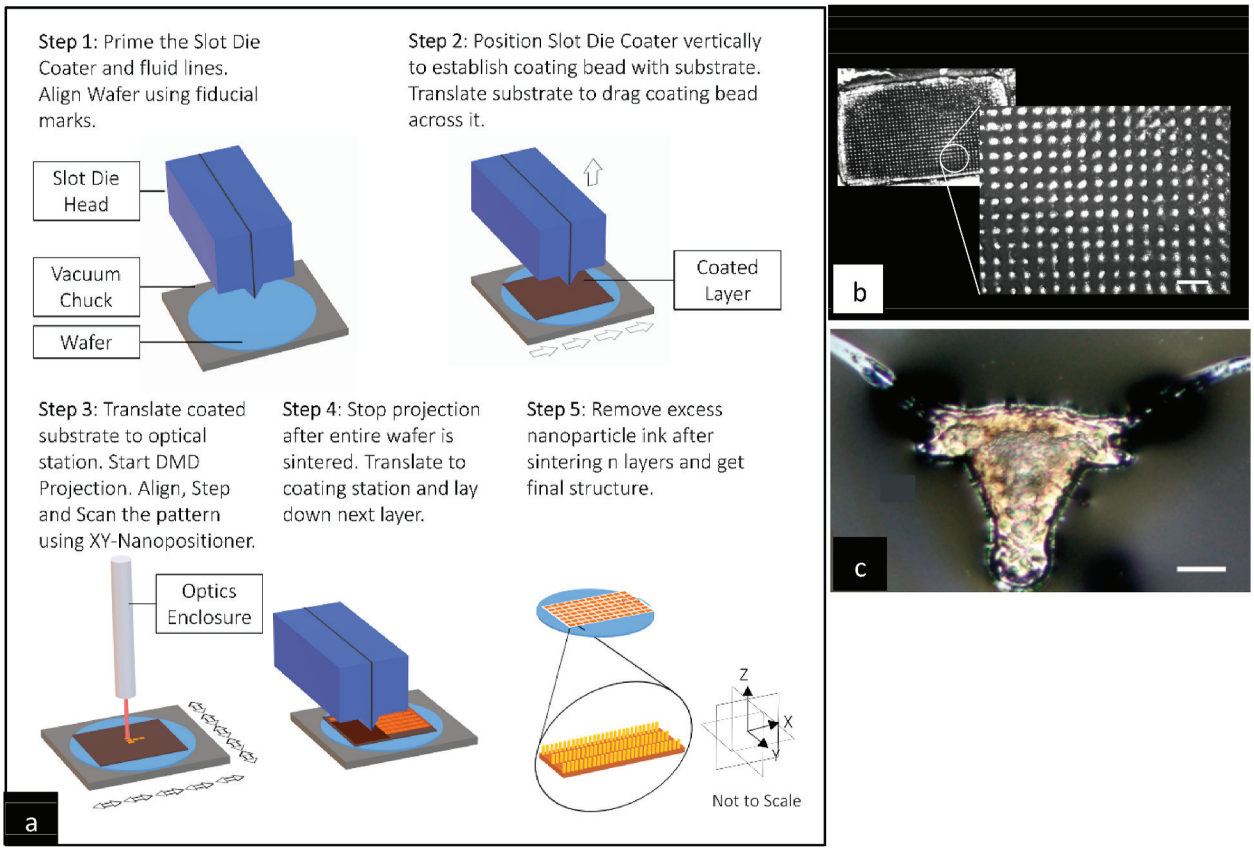

Fig. 4. (a) Simplified step-by-step schematic of the μ-SLS process. (b) An optical microscope image showing the full areal scale (2.3 mm × 1.2 mm) array sintered on a 1 μm thick Ag NP ink layer. (inset) Enlarged image of an array of 20 μm diameter circles with 40 μm pitch. (c) Optical microscope image of longhorn logo (trademark of The University of Texas at Austin). The smallest feature size in this sintered part is around 7 μm near the tip of the longhorn ears.

form of NPs with narrow size distributions are required. However, as the particle diameters are scaled down to the nanoscale, agglomeration of the particles becomes a significant issue due to the enhanced effect of van der Waals forces at these scales [108,109]. To reduce this agglomeration problem, the μ-SLS process uses NP inks with surfactant coatings, which are burned off during the sintering step, to prevent agglomeration of the particles during the coating step [107]. Initial studies of the μ-SLS process have mainly used Cu and Ag nanoparticle (NP) inks to fabricate high complexity 2.5D parts and demonstrate the capability to produce 3D microparts [106,110,111]. However, the current iteration of the μ-SLS tool can process almost any metallic and polymeric materials which can be suspended in the form of a NP inks.

One of the key materials challenges in μ-SLS is the sintering of ceramic materials. This is because nanoceramics often suffer from inhomogeneous particle agglomeration, early onset of sintering due to lower activation energy compared to micron-scale ceramic particles, and a wider distribution of particles due to ineffective nanoparticle separation techniques compared to metal and polymer NPs [112]. While lower activation energy can be perceived as an advantageous proposition in lowering the sintering energy required, when coupled with the uneven distribution and packing of these nanoparticles it becomes difficult to control grain growth. Controlling sintering schedules, introducing grain growth suppressants, driving sintering through isostatic pressing, and coupling densification and superplastic deformation techniques (like forging) at high temperatures are some strategies used to mitigate the problems associated with nanoceramic sintering. However, both of these pressure-less and pressure-based sintering methods are slow and unable to process complex structures. Therefore, major challenges still exist in producing ceramic parts using μ-SLS.

5.2.2. *Possible approaches to overcome materials challenges for μ-SLS*

A potential approach which can be integrated with the μ-SLS process to improve consolidation of semiconductor nanoceramics and achieve higher densification rates is the use of a field-assisted laser flash sintering (FS) technique. In conventional FS techniques, an electric field (1–1000 V/cm) is applied directly to the green part causing effective rapid sintering. While the most widely accepted explanation of the fundamental physical phenomenon behind FS is Joule-heating runaway, researchers have yet to confirm that hypothesis with strong experimental evidence covering a range of ceramic materials [112,113]. Although FS has revolutionized the production scale fabrication of macroscale ceramic structures, there are challenges associated with the effective localization of sintering energy, uneven grain growth and avoidance of thermal shock. Hagen et al. [114] demonstrated the idea of Laser Flash Sintering (LFS) of nanoceramics in a layer-by-layer manner by simultaneously use of a galvanometric laser scanner and pulsed electric field to initiate necking between the particles. The laser facilitates the formation of necks between the selectively exposed nanoparticles at significantly lower temperatures and times, eliminating thermal shocks. The strength of the partially sintered particles is significant enough to effectively separate them from the un-sintered particles without affecting part fidelity, and conventional or flash sintering approaches can then be used to achieve full densification of the part. LFS could potentially be used in conjunction with a μ-SLS framework without major modifications to the process to improve its ability to fabricate ceramic parts.

5.3. 3D feature fabrication

5.3.1. Capabilities and challenges in μ-SLS for fabricating 3D features

The μ-SLS process can currently produce multilayer 2.5D structures on a 50 mm wafer. In principal, there should be few limitations to the types of structures and overhangs that μ-SLS can produce since unsintered NPs in the μ-SLS bed act as a support structure during the build process. In fact, the only major limitation should be the fabrication of closed structures, such as hollow spheres, where the unsintered NPs cannot be removed from the inside of the part during post processing. There are, however, practical challenges in fabricating true-3D structures with μ-SLS which must be addressed in order to fabricate true 3D parts with the process. Avoiding residual thermal stresses that can warp the final part and improving control over interlayer fusion are central to achieving this capability.

5.3.2. Possible approaches to overcome 3D feature fabrication challenges in μ-SLS

Thermal stresses in sintered parts can be reduced by decreasing the magnitude of the thermal gradient across the bed through uniform heating of the deposited NPs. A conventional hot-plate heating technique is used to partially dry the NP layers in the μ-SLS process, but the non-uniform energy exposure densities leads to drying of each section at varying rates [115]. To achieve precise partial drying of the NP layers, a uniform energy exposure density on the surface could be maintained by using an infrared emitter. This would allow each layer to be more uniformly heated and dried, which could reduce thermal gradients in the fabrication process, and thus the residual thermal stresses in the final part, resulting in more accurate 3D builds.

Another approach to improving 3D feature control in μ-SLS is through advanced process control including process monitoring and in-situ metrology techniques coupled with closed loop feedback. However, the extremely wide parameter space for optimizing μ-SLS and dearth of accurate models of the μ-SLS process have limited ability to implement advance process control. Integrating vision, temporal, and thermal metrology systems that can detect material and process abnormalities in the μ-SLS process can both improve understanding of the μ-SLS process and allow for more accurate fabrication of 3D structures. That said, the high process area to spatial feature size ratio (~10000:1) in the μ-SLS process presents significant challenges in yielding useful in-situ optical or thermal information, as there's an inherent trade-off between field-of-view and resolution for these measurement techniques. In addition, to make optimal use of in-situ metrology advanced models of the nanoscale laser-material interactions must be developed to better understand the underlying physics behind the process. These models can help in understanding NP consolidation mechanisms and predicting the mechanical and thermal properties of fabricated 3D structures. This would provide valuable information about key process parameters like coating thickness and laser irradiance [116]. As such, the overall 3D part production capability of the μ-SLS process can be improved by reducing thermal gradients during sintering and employing advanced process control techniques to monitor *in-operando* part fabrication quality. However, completely closed hollow structures with thin walls would be almost impossible to produce, given the design constraints of the process.

5.4. Feature size resolution

5.4.1. Feature size resolution capabilities and challenges for μ-SLS

Parts with minimum feature size of sub-10 μm have been fabricated using the μ-SLS process [117,118]. The lateral resolution of the μ-SLS process is limited primarily by the heat diffusion away from the laser focal spot when exposure durations are high. This thermal diffusion creates heat-affected zones (HAZs) around the intended part which result in poor control over net-shaped features and unacceptable surface roughness. The vertical resolution of the process is controlled by slot die coated layer thickness and the laser thermal penetration depth which varies with the composition of the NP bed as well as the laser wavelength and intensity.

5.4.2. Possible approaches to overcome current limits in feature size resolution for μ-SLS

The HAZs in μ-SLS can be reduced by lowering laser exposure duration and increasing laser power to limit the heat transfer away from the laser spot. Previous results have shown that use of nano and femtosecond lasers significantly decreases the HAZs but produces much narrower processing windows for nanoparticle sintering due to the very small difference in the sintering and melting exposure thresholds [119]. The HAZs and feature size resolution of μ-SLS can be further improved by using optical proximity correction algorithms, like the ones commonly used in nanolithography, to account for image distortions caused by heat or light spreading from the intended feature exposure area [120]. Through such algorithms and by reducing the exposure time/increasing the exposure power, it should be possible to achieve a lateral resolution in μ-SLS that is close to the diffraction limit of the laser light used to pattern the structures.

The optical penetration depth, which determines the vertical resolution of the μ-SLS process, is dependent on the laser wavelength and dwell time, and the thermal diffusivity of the substrate. Therefore a better understanding of the nanoscale transport mechanisms in μ-SLS is critical to creation of accurate nanoparticle sintering models, and thus achieving higher resolution, true-3D parts with μ-SLS [116]. Typical laser penetration depths range from a few hundred nanometers to tens of micrometers depending on the laser wavelength and exact NP composition for metal nanoparticles in the visible spectrum [119,121]. Therefore, the likely limit of the resolution of μ-SLS in the vertical direction lies in the range of a few hundred nanometers if accurate opto-thermal models of the μ-SLS process can be created and used to optimize the build process.

5.5. Throughput

5.5.1. Throughput capabilities and challenges for μ-SLS

The maximum demonstrated volumetric fabrication throughput of the μ-SLS process is currently ~63 mm^3/h [117,118]. Features of the μ-SLS system which can limit throughput are the coating speed, nanopositioner alignment and settling times, sintering exposure time, and the inherent scalability tradeoffs between resolution and throughput. The current throughput budget of the μ-SLS process is determined in large part by the efficiency of the sintering process and speed of the slot die coating mechanism. The current sintering time of the μ-SLS system is 100 ms per exposure which includes a 50 ms laser exposure time and a 50 ms stepping time. The exposure time can likely be decreased by increasing the exposure power and the stepping time improved by reducing settling time of the nanopositioning stages used [122]. A coating speed of 1 mm/s is currently used for the slot die coating process to ensure uniform coating layers, but this time may also be improved by optimizing the coating process parameters.

5.5.2. Possible approaches to overcome current throughput limits in μ-SLS

Currently, a 50 mm wafer can be sintered using the μ-SLS process in ~140 s. Of these 140 s, the travel time between coating station and optical station, which includes the NP ink deposition and partial ink drying as well as the homing of the stage under the optical subsystem, consumes ~60 s. Over 90% of this budget is allocated to the coating time, which depends on the flow rate inside slot die coater, layer thickness resolution and material rheological properties (specifically, Ca number). The deposition time can be experimentally optimized by identifying a coating window for a range of Ca numbers, slot-die speeds and bed thickness, with the objective of achieving a uniform coating with minimal variation along the direction of motion. Recent results have shown that uniform coatings can be produced with NP inks at ~15

mm/s coating speeds [123] and the drying time could be reduced to ~2 s which would reduce the coating and travel time between substations to ~10s.

The total time currently needed to sinter one complete NP layer on the wafer is ~80 s, limited by sintering exposure duration and settling time of the nanopositioning stages. This can be reduced by using higher power lasers which can achieve the similar densification quality at shorter exposure durations. The settling time of the nanopositioner steps can be improved by applying better control strategies to reduce the overshoot during tracking. It is estimated that both the exposure time and the settling times of the stages could be reduced to ~10 ms which would reduce the overall sintering time to ~16 s. With these assumptions the volumetric throughput of the μ-SLS system could be increased to a theoretical maximum of ~340 mm^3/h with a layer thickness of 1 μm. Therefore, the overall fabrication time for a 10:1 aspect ratio structure with a vertical and lateral resolution of 1 μm could be reduced to a build time of less than 10 min, including the excess material removal and post-processing steps assuming the optimized μ-SLS process parameters. Further improvements in the volumetric throughput could be achieved by increasing the layer thickness, albeit at the proportional cost to the vertical part resolution.

5.6. Prognoses

The μ-SLS process is a high throughput microscale metal AM process with a minimum resolution of 1 μm. The true-3D fabrication capabilities of the process have not been demonstrated yet due to challenges associated with uniform layer deposition and laser penetration depths, and the approaches discussed in section 6.3.2 are under development. The fundamental limitation to feature geometry using μ-SLS process is in the creating hollow spheres as the nanoparticle ink inside the sphere cannot be reliably removed in the post-processing steps.

6. Assembling micro/nanocomponents using Holographic Optical Tweezing

6.1. Description of the Holographic Optical Tweezing process

Optical tweezing is a method for spatial confinement and manipulation of spherical and non-spherical particles on the micro- and nanoscale using radiation pressure from focused laser beams. The technique was first demonstrated in 1970 by Arthur Ashkin [124], who later matured the field [125–127] and received the 2018 Nobel Prize in physics for his revolutionary invention. The optical tweezers (OT) approach, also known as optical trapping, uses a laser beam that is tightly focused by a high numerical aperture (NA) objective lens. When the beam's focal point interacts with a micro- or nano-scale particle, various mechanisms can produce a stable potential well at the beam's focus. In the Rayleigh (or wave optics) regime, absorptive [128] or transparent [129] particles with $D < \lambda/10$ (where D is the particle diameter and λ is the wavelength of the focused laser beam) can be treated as dipoles in an electric field. In the ray tracing regime ($D > 10^* \lambda$), transparent particles with diameters larger than λ/10 experience trapping forces that primarily arise from momentum transfer during refraction [130]. In the Mie regime ($\lambda/10 < D < 10^* \lambda$), trapping forces result from a more complicated scattering behavior between microparticles and photons [131]. In all regimes, movement of the beam's focus in either lateral or axial directions allow for stably trapped particles to be positioned in three-dimensional space.

The most common approach for scaling OT to handle multiple particles simultaneously is the holographic optical tweezers (HOT) approach [132], which uses a diffractive optical element (DOE) [133] to split and/or modulate a single laser beam. The most common DOE used in the HOT approach is a computer-controlled spatial light modulator (SLM) [134], which enables dynamic and real-time wavefront shaping. Several numerical algorithms exist to calculate phase-only holograms in real-time [135] and the most common is the standard Gerchberg-Saxton phase retrieval algorithm [136]. Fig. 5 shows the schematic of HOT and 3D features assembled using this process.

6.2. Materials

6.2.1. Materials capabilities and challenges in optical tweezing

The OT and HOT approaches have been used to handle micro- and nano-particles of a variety of optically transparent materials including silica [138], polystyrene [134], and polymethyl methacrylate (PMMA) [139]. Handling of absorptive ceramic or reflective metallic microparticles has been demonstrated but is more challenging due to the complex light fields required to produce stable trapping forces [140].

6.2.2. Possible approaches to overcome materials challenges for optical tweezing

OT has proven to be most effective at manipulating colloidal particles under certain conditions. First, most optical trapping occurs within an aqueous suspension where gravitational forces are offset by buoyancy, although trapping in air is also possible [141]. Furthermore, the strongest optical traps have been demonstrated with transparent microparticles (e.g., PS, PMMA, or silica) that have high refractive indices relative to their suspension medium [142]. However, optical tweezing of almost any dielectric or conductive microparticle is theoretically possible by utilizing more sophisticated structured light fields (e.g., optical vortices [143] or counter-propagating traps [144]) that operate based on optical momentum transfer from reflection or absorption rather than refraction. Metal nanoparticles can be manipulated by certain wavelengths due to unique optical properties originating from resonances in the light scattered by the particle [145].

6.3. 3D feature fabrication

6.3.1. Capabilities and challenges in optical tweezing for fabricating 3D features

Optical tweezers exhibit stronger forces in the radial direction (i.e., in the beam's focal plane) than the axial direction (i.e., along the beam propagation direction) [142], so special considerations are required when scaling from fabrication of two-dimensional assemblies to true three-dimensional structures. Like in many common additive manufacturing approaches, optical tweezers are adaptable to layer-by-layer addition [146]. Although the OT approach fundamentally allows for simultaneous handling of multiple particles across 3D space, it has not yet been shown to be a feasible alternative to layer-by-layer processing [147]. Closed-loop control based on image feedback [148–150] provides a promising path towards unsupervised assembly of 2D layers or 3D structures, however the shallow depth-of-field of high-NA microscope objectives makes detection of out-of-focal-plane particles challenging. Furthermore, if the system's microscope objective is not index-matched to the medium (e.g. in the case of a high-NA oil immersion objective trapping in an aqueous, non-oil medium), then spherical aberrations accumulate with increased trapping depth and reduce the amount of optical trapping force [151].

6.3.2. Possible approaches to overcome 3D feature fabrication challenges in optical tweezing

Currently, the largest challenge in fabricating permanent 3D structures of microparticles in a layer-by-layer approach is the additional process required for permanent joining. Various methods have been proposed for this purpose such as melting particles at their interfaces [152], optical tweezing in a liquid pre-polymer medium and joining via one- [153] or two-photon [154] photopolymerization reactions, and surface functionalization of particles with bio-molecules like biotin and streptavidin [155]. Another assembly approach involves the use of complementary sets of building-block microparticles, including those that can be attached together to make reconfigurable structures

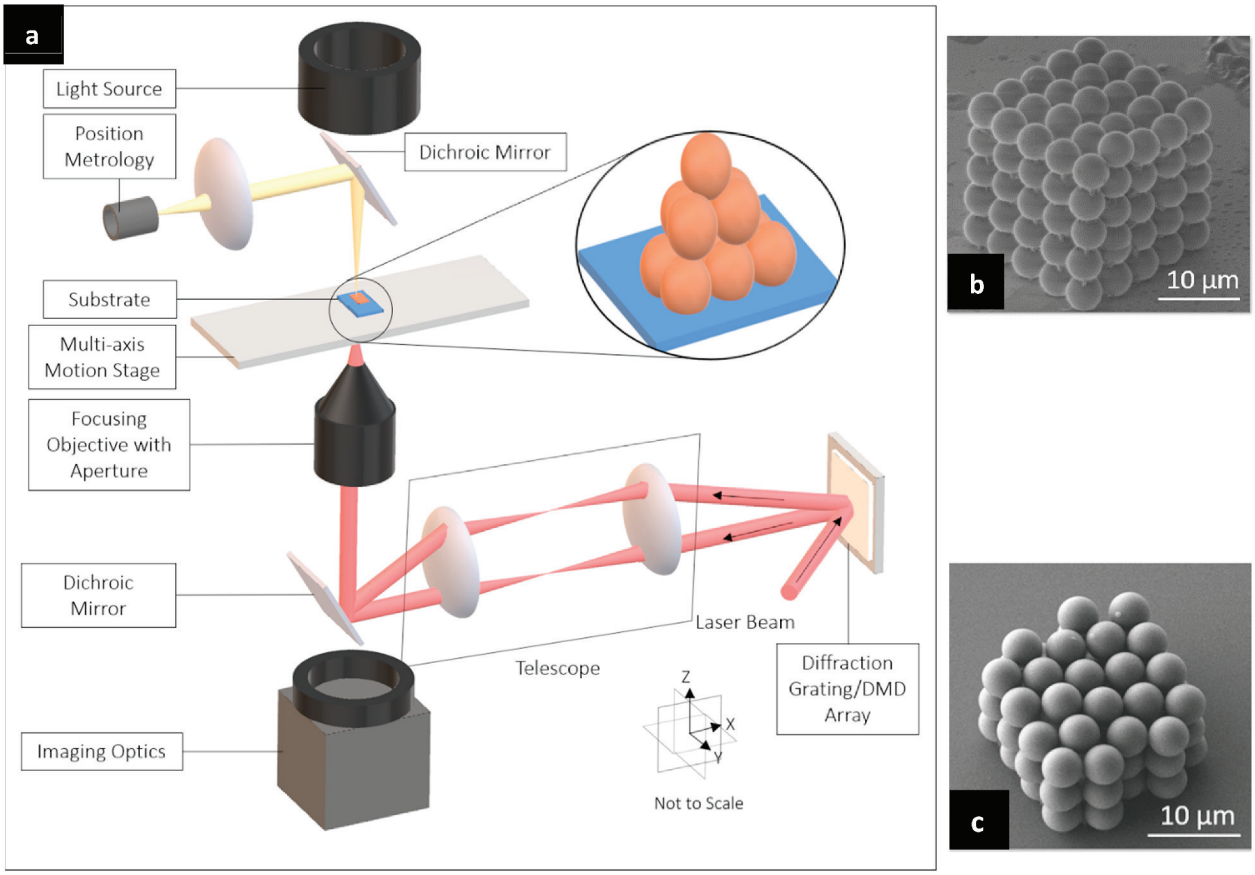

Fig. 5. (a) Schematic diagram of a typical the holographic optical tweezers system, figure reprinted from Ref. [134]. The incoming laser beam is split into several beams using a diffractive optical element and then focused on to the sample plane to spatially confine and manipulate micro/nanoscale particles at the points where they have been focused. The assembled particles can be further cured into 3D structures using localized heating or single/two-photon photopolymerization steps. (b, c) SEM images of 3D silica assemblies created by OT, figure reprinted from Ref. [137].

[156–158] or snap-fit-like permanent fixtures [159]. Considering the strengths and limitations of the aforementioned approaches, highly-localized two-photon photopolymerization of a liquid pre-polymer medium currently allows for the most controlled and scalable way to additively manufacture microstructures [137,160].

Furthermore, the HOT approach holds the potential to augment other microfabrication techniques such as multiphoton lithography [160]. This combination results in a versatile system that can fabricate microparticles or microstructures, manipulate them into 3D configurations using optical forces, and permanently join them with polymer [161], metals [24,162], or ceramics [163–165]. Such an approach has been demonstrated in work by Chizari et al. that used HOT to assemble a $5 \times 5 \times 5$ granular silica crystal and joined them by two-photon polymerization (TPP) of the surrounding medium(Fig. 5b) [137]. Work by Askari [166] also shows the combination of OT with TPP to create layered structures with microspheres and polymer. Chizari et al. [161] recently demonstrated a combination of the HOT and TPP approaches that produces microstructures with embedded strain energy.

6.4. Feature size resolution

6.4.1. Feature size resolution capabilities and challenges for optical tweezing

Holographic optical tweezers have been used to precisely locate particles as small as 5 nm[132] and as large as 60–75 µm [161,167] in both two- [134] and three-dimensions [168]. Automated handling of 100 particles with average velocity of 15 µm/s per particle was recently reported [148]. Brownian motion limits the positioning accuracy of microparticles to approximately 350 nm within a room-temperature aqueous medium [169], although a colder and more viscous medium would have improved accuracy [170]. OT has also been demonstrated viscous media up to $\eta = 2000$cP [171] including ethylene glycol [172] gelatin [147] and various pre-polymer solutions [153] which can offer reduced Brownian motion and higher heat capacity. All HOT systems and virtually all optical imaging systems are limited in resolution to a few hundred nanometers by the optical diffraction limit, $d = \lambda/(2*NA)$, where d is the size of the minimum resolvable distance, λ is the illumination wavelength, and NA is the numerical aperture of the objective lens.

6.4.2. Possible approaches to overcome current limits in feature size resolution for optical tweezing

Recent developments in creating precisely shaped nano-particles have shown promise for increasing optical trapping forces and dexterity at smaller scales via non-photonic interactions (e.g., plasmonic interactions [173,174] or whispering-gallery mode resonances [175]). A recent study has also reported possibility of optical manipulation of macroscale objects by controlling the refraction of light via adding subwavelength nanophotonic structures on their surfaces [176]. However, imaging increasingly smaller particles becomes challenging beyond the diffraction limit of light. Super-resolution, or sub-diffraction-limited, imaging techniques have been demonstrated outside of OT systems [177], although considerable development is needed before these approaches can be used with the OT approach.

6.5. Throughput

6.5.1. Throughput capabilities and challenges for optical tweezing

The HOT approach allows for additive fabrication of complex multi-material structures by using microparticles as the building blocks. Therefore, this method is a promising approach to fabricate micro-granular crystals (i.e., nonlinear metamaterials consisting of closely-packed arrays of particles [178]) with any desired 3D bulk shape and controlled vacancy locations, a capability which is not possible with established self-assembly approaches [179]. It is estimated that automated HOT can yield 3D microgranular crystals with volumetric rate of 3.7 mm^3/h in the foreseeable future [137]. The HOT approach throughput relies on the maximum speed that each particle can be moved and the maximum number of particles that can be concurrently patterned into shapes. In addition to particle positioning, the time required for particle delivery and permanent joining also affect the throughput of this approach.

6.5.2. Possible approaches to overcome current throughput limits in optical tweezing

As discussed above, throughput of OT as a fabrication method depends on a variety of parameters. For an ideal optical tweezers system, the ultimate drag velocity of the particles is limited by power per trap, which is set by the maximum incident power threshold of the SLM. Potential improvements in liquid crystal materials or alternative beam shaping techniques such as use of dynamic micromirrors [180] can result in an increase in maximum incident power, and thereby throughput. Further process improvements to the suspension fluid, particle delivery system, parallelized optical columns, and substrate nanopositioning systems may allow for step-and-repeat manufacturing at increased throughputs. In the case of combining optical tweezing with two-photon polymerization, the overall fabrication throughput can be improved by parallelization of the polymerization process which is discussed in detail in section 8.5.

6.6. Prognoses

Optical tweezing has proven to be a very powerful approach for manipulation of meso-, micro-, and nanoscale objects. Its resolution, dexterity with a variety of particle shapes, and multimaterial capabilities make it a promising technique for microscale applications where precision is of utmost importance. For example, the OT approach provides a means to enable the fabrication of microgranular crystals, which hold potential for use in a wide variety of application such as a shock-absorbing metamaterial [181], photonic crystals [182] and acoustic lenses [183]. However, scalability of this technique for the fabrication of bulk materials is still a challenge mainly because of its throughput limitations. Further technological improvements in the fabrication system components such as SLMs, galvanometers, and pulsed lasers will increase the throughput of optical tweezing as a high-resolution AM technique.

7. Conclusions

This article is the second one in a four-part series of articles which discuss the challenges associated with microscale additive manufacturing processes. Laser-based microscale AM processes are ubiquitous in the macroscale feature-size (>100 μm) market which has applications in defense, aerospace, and rapid prototyping industry. Because of the wide energy densities that are available with lasers, several controllable interaction mechanisms in metals, semiconductors, insulators and polymers have been investigated which can be leveraged for micro-nanoscale fabrication. As part of this article, the material, resolution, geometry and throughput constraints for laser-based microscale AM processes have been explored, and potential solutions to specific issues have been comprehensively discussed. Micro-Stereolithography is one of the first microscale AM processes that was developed. μ-SLA uses a single-photon absorption mechanism and its variants are reliably able to produce sub-5 μm parts. However, there are several challenges associated with fabricating higher resolution parts using a single photon photopolymerization approach. Therefore, two-photon or multi-photon absorption approaches (TPL) have been investigated to create the part inside the reactive medium in a voxel-by-voxel manner. TPL offers several advantages over other microscale AM approaches including higher resolution, throughput and better geometric capabilities. Optical tweezing-based approaches are used to manipulate and precisely position individual particles into 3D structures which can then be permanently joined using multiphoton lithography approaches. However, these laser curing approaches are generally limited by the materials which can be polymerized. Laser heating processes like LIFT and μ-SLS are designed for a wider range of materials. While LIFT uses localized heating to transfer material on to the substrate due to shearing or cavitation pressure, μ-SLS consolidates thin material films by localized necking to form 3D parts in a layer-by-layer manner. The achievable resolution using these processes is currently limited to sub-10 μm. However, the potential to parallelize the process, achieve true-3D geometries and create metallic structures make LIFT and μ-SLS strong candidates for microfabrication. The limitations to the scalability of these processes have been discussed and potential approaches to mitigate the challenges have been proposed. A comprehensive overview of general design principles that must be followed while developing laser-based microscale AM processes are presented in part IV of the series of articles.

Contributions

The following contributions were made by the authors associated with this article. DB and MC reviewed and wrote the section on LIFT. DB, NR, LC and MC reviewed and wrote the section on μ-SLS. SC, LH, MP, JH reviewed and wrote the sections in Optical Tweezing. RH, ZX and XZ reviewed and wrote the sections on μ-SLA. SS reviewed and wrote the section on TPL. DB and MC reviewed and edited the manuscript.

Declaration of competing interest

The authors declare that they have no known competing financial interests or personal relationships that could have appeared to influence the work reported in this paper.

Acknowledgements

This series of publications is a joint effort by the members and affiliates of the Micro-Nano Technical Leadership Committee of the American Society for Precision Engineering (ASPE). This work was supported in part by AFOSR under award number FA9550-18-1-0459 and by Prof. Hopkins' DOE-nominated Presidential Early Career Award for Scientists and Engineers under award number B620630."

References

[1] Behera D, Cullinan MA. Current challenges and potential directions towards precision microscale Additive manufacturing – Part I: direct ink writing/jetting processes. *Precis. Eng.* **Submitted** 2020.
[2] Chizari S, Shaw LA, Behera D, Roy NK, Zheng X, Panas RM, et al. Current challenges and potential directions towards precision microscale Additive manufacturing – Part III: energy induced deposition and hybrid electrochemical processes. Precis. Eng. 2021;68:174–86.
[3] Bhattacharjee N, Parra-Cabrera C, Kim YT, Kuo AP, Folch A. Desktop-stereolithography 3D-printing of a poly(dimethylsiloxane)-based material with sylgard-184 properties. Adv Mater 2018;30.
[4] Patel DK. Highly stretchable and UV curable elastomers for digital light processing based 3D printing. Adv Mater 2017;29:1606000.
[5] Chen S. Nanomanufacturing. American Scientific Publishers; 2009.

[6] Zheng X, et al. Design and optimization of a light-emitting diode projection micro-stereolithography three-dimensional manufacturing system. Rev Sci Instrum 2012;83.
[7] Tumbleston JR. Continuous liquid interface production of 3D objects. Science 2015;347(80-):1349–52.
[8] Chen D, Zheng X. Multi-material additive manufacturing of metamaterials with giant, tailorable negative Poisson'. *s ratios*. Sci Rep 2018;8:9139.
[9] Cui H, Hensleigh R, Chen H, Zheng X. Additive Manufacturing and size-dependent mechanical properties of three-dimensional microarchitected, high-temperature ceramic metamaterials. J Mater Res 2018;33:360–71.
[10] Kuang X. High-speed 3D printing of high-performance thermosetting polymers via two-stage curing. Macromol Rapid Commun 2018;39:1700809.
[11] Hegde M. Printing all-aromatic polyimides using mask-projection stereolithography: processing the nonprocessable. *Al*vol. 3; 2017. p. 1701240.
[12] Ge Q. Multimaterial 4D printing with tailorable shape memory polymers. Sci Rep 2016;6:31110.
[13] Ji Z, Yan C, Yu B, Wang X, Zhou F. Multimaterials 3D printing for free assembly manufacturing of magnetic driving soft actuator. Adv. Mater. Interfaces 2017;4:1700629.
[14] Zarek M. Printing of shape memory polymers for flexible electronic devices. *Al*vol. 3; 2016. p. 4449–54.
[15] Eckel ZC. Additive manufacturing of polymer-derived ceramics. Science (80-.) 2016;351:58–62.
[16] Kotz F. Three-dimensional printing of transparent fused silica glass. Nature 2017;544:337–9.
[17] Hensleigh M. R. Additive manufacturing of complex micro-architected graphene aerogels. Mater. Horiz 2018;5:1035–41.
[18] Zheng X. Ultralight, ultrastiff mechanical metamaterials. Science (80-.) 2014;344:1373–7.
[19] Zheng X. No Title. *al.* Multiscale Met. metamaterials. Nat. Mater 2016;15:1100–6.
[20] Bauer J Nanolattices. An emerging class of mechanical metamaterials. Adv Mater 2017;29:1701850.
[21] Fantino E. 3D printing of conductive complex structures with in situ generation of silver nanoparticles. Adv Mater 2016;28:3712–7.
[22] Cui H. Three-dimensional printing of piezoelectric materials with designed anisotropy and directional response. Nat Mater 2019;18.
[23] Yao D, et al. Achieving the upper bound of piezoelectric response in tunable , wearable 3D printed nanocomposites. Adv Funct Mater 2019:1–11. 1903866.
[24] Vyatskikh A, et al. Additive manufacturing of 3D nano-architected metals. Nat Commun 2018;9:593.
[25] Pan Y, He H, Xu J, Feinerman A. Study of separation force in constrained surface projection stereolithography. Rapid Prototyp J 2017;23:353–61.
[26] Lambert PM, Iii EAC, Williams CB. Design considerations for mask projection microstereolithography systems. In: Solid freeform fabrication symposium; 2013.
[27] Jiang J, Xu X, Stringer J. Support structures for additive manufacturing: a. Rev. J. Manuf. Mater. Process 2018;2.
[28] Wu L. Bioinspired ultra-low adhesive energy interface for continuous 3D printing: reducing curing induced adhesion. Research 2018:1–10.
[29] Zheng X. Design and optimization of a light-emitting diode projection micro-stereolithography three-dimensional manufacturing system. Rev Sci Instrum 2012;83:125001.
[30] Scott TF, Kowalski BA, Sullivan AC, Bowman CN, McLeod RR. Two-color single-photon photoinitiation and photoinhibition for subdiffraction photolithography. Science (80-.) 2009;324:913–7.
[31] Fourkas JT, Petersen JS. 2-Colour photolithography. Phys Chem Chem Phys 2014;16:8731–50.
[32] Zhou C, Ye H, Zhang F. A novel low-cost stereolithography process based on vector scanning and mask projection for high-accuracy, high-speed, high-throughput, and large-area fabrication. J Comput Inf Sci Eng 2015;15:11003.
[33] Sun H-B, Kawata S. Two-photon photopolymerization and 3D lithographic microfabrication. Adv Polym Sci 2004:169–274.
[34] Saha SK, et al. Scalable submicron additive manufacturing. Science (80- 2019;366:105–9.
[35] Maruo S, Nakamura O, Kawata S. Three-dimensional microfabrication with two-photon-absorbed photopolymerization. Opt Lett 1997;22:132.
[36] Malinauskas M, Žukauskas A, Bičkauskaitė G, Gadonas R, Juodkazis S. Mechanisms of three-dimensional structuring of photo-polymers by tightly focussed femtosecond laser pulses. Optic Express 2010;18:10209.
[37] Fischer J, et al. Three-dimensional multi-photon direct laser writing with variable repetition rate. Optic Express 2013;21:26244–60.
[38] Sun HB, Kawata S. Two-photon laser precision microfabrication and its applications to micro - nano devices and systems. J Lightwave Technol 2003;21:624–33.
[39] Saha SK, et al. Radiopaque resists for two-photon lithography to enable submicron 3D imaging of polymer parts via X-ray computed tomography. ACS Appl Mater Interfaces 2018;10:1164–72.
[40] Jiang L, et al. Performance comparison of acrylic and thiol-acrylic resins in two-photon polymerization. Optic Express 2016;24:13687.
[41] Quick AS, et al. Rapid thiol-yne-mediated fabrication and dual postfunctionalization of micro-resolved 3D mesostructures. Adv Funct Mater 2015;25:3735–44.
[42] Harnisch E, et al. Optimization of hybrid polymer materials for 2PP and fabrication of individually designed hybrid microoptical elements thereof. Opt Mater Express 2015;5:456.
[43] Vyatskikh A, et al. Additive manufacturing of 3D nano-architected metals. Nat Commun 2018;9:593.
[44] Xiong W, et al. Laser-directed assembly of aligned carbon nanotubes in three dimensions for multifunctional device fabrication. Adv Mater 2016;28:2002–9.
[45] Obata K, El-Tamer A, Koch L, Hinze U, Chichkov BN. High-aspect 3D two-photon polymerization structuring with widened objective working range (WOW-2PP). Light Sci Appl 2013;2:1–5.
[46] Saha SK, Divin C, Cuadra JA, Panas RM. Effect of proximity of features on the damage threshold during submicron additive manufacturing via two-photon polymerization. J Micro Nano-Manufacturing 2017;5:031002.
[47] Rumi M, et al. Structure - property relationships for two-photon absorbing chromophores: bis-donor diphenylpolyene and bis(styryl)benzene derivatives. J Am Chem Soc 2000;122:9500–10.
[48] Bauer J, Schroer A, Schwaiger R, Kraft O. Approaching theoretical strength in glassy carbon nanolattices. Nat Mater 2016;15:438–43.
[49] Crook C, et al. Plate-nanolattices at the theoretical limit of stiffness and strength. Nat Commun 2020;11:1–11.
[50] Zhang X, et al. Theoretical strength and rubber-like behaviour in micro-sized pyrolytic carbon. Nat Nanotechnol 2019;14.
[51] Bauer J, et al. Additive manufacturing of ductile, ultrastrong polymer-derived nanoceramics. Matter 2019;1:1547–56.
[52] Oakdale JS, et al. Direct laser writing of low-density interdigitated foams for plasma drive shaping. Adv Funct Mater 2017;27:1–10.
[53] Lu WE, Dong XZ, Chen WQ, Zhao ZS, Duan XM. Novel photoinitiator with a radical quenching moiety for confining radical diffusion in two-photon induced photopolymerization. J Mater Chem 2011;21:5650–9.
[54] Xing JF, et al. Improving spatial resolution of two-photon microfabrication by using photoinitiator with high initiating efficiency. Appl Phys Lett 2007;90:1–4.
[55] Yang L, et al. Parallel direct laser writing of micro-optical and photonic structures using spatial light modulator. Optic Laser Eng 2015;70:26–32.
[56] Hahn V, et al. Rapid assembly of small materials building blocks (voxels) into large functional 3D metamaterials. Adv Funct Mater 2020;1907795.
[57] Mills B, Grant-Jacob JA, Feinaeugle M, Eason RW. Single-pulse multiphoton polymerization of complex structures using a digital multimirror device. Optic Express 2013;21:14853.
[58] Shugaev MV, Bulgakova NM. Thermodynamic and stress analysis of laser-induced forward transfer of metals. Appl Phys A Mater Sci Process 2010;101:103–9.
[59] Morales M, Marquez A, Lauzurica S. Laser-induced forward transfer techniques and applications. In: Advances in laser materials processing. vols. 339–379. Elsevier Ltd.; 2018. https://doi.org/10.1016/B978-0-08-101252-9.00013-3.
[60] Delaporte P, Alloncle A. Laser-induced forward transfer : a high resolution additive manufacturing technology. Optic Laser Technol 2016;78:33–41.
[61] Piqu A, Auyeung RCY, Kim H, Charipar NA, Mathews SA. Laser 3D micro-manufacturing. 2016. https://doi.org/10.1088/0022-3727/49/22/223001.
[62] Zenou M, Kotler Z. Printing of metallic 3D micro-objects by laser induced forward transfer. Optic Express 2016;24:1431.
[63] Bohandy J, Kim BF, Adrian FJ. Metal deposition from a supported metal film using an excimer laser. J Appl Phys 1986;60:1538–9.
[64] Willis DA, et al. Printing of silver conductive lines through laser-induced forward transfer. Appl Surf Sci 2017;254:1–4.
[65] Kuznetsov AI, Kiyan R, Chichkov BN. Laser fabrication of 2D and 3D metal nanoparticle structures and arrays. Optic Express 2010:127–32. 21198.
[66] Papakonstantinou P, Vainos NA, Fotakis C. Microfabrication by UV femtosecond laser ablation of Pt , Cr and indium oxide thin films. Appl Surf Sci 1999;151:159–70.
[67] Zenou M, Sa'ar A, Kotler Z. Digital laser printing of aluminum micro- structure on thermally sensitive substrates. J Phys D Appl Phys 2015;48.
[68] Mattle T, Shaw-stewart J, Schneider CW, Lippert T, Wokaun A. Laser induced forward transfer aluminum layers : process investigation by time resolved imaging. Appl Surf Sci 2012;258:9352–4.
[69] Tóth Z, Szörényi T. Pulsed laser processing of Ge/Se thin film structures. Appl. Phys. A Solids Surfaces 1991;52:273–9.
[70] Ollinger M, Kim H, Sutto T, Martin F, Piqué A. Laser direct-write of polymer nanocomposites. J. Laser Micro Nanoeng. 2006;1:102–5.
[71] Thomas B, et al. Experimental investigations of laser-induced forward transfer process of organic thin films. Appl Surf Sci 2007;254:1206–10.
[72] Arnold CB, Serra P, Piqué A. Laser direct-write techniques for printing of complex materials. MRS Bull 2011;32:23–32.
[73] Fogarassy E. Basic mechanisms and application of the laser-induced forward transfer for high-T c superconducting thin film deposition. Prog. High-Temperature Supercond. Transistors Other Devices 1990;1394:169.
[74] Pique A, Auyeung RCY, Kim H, Charipar NA, Mathews SA. Laser 3D micro-manufacturing. J Phys D Appl Phys 2016;49.
[75] Fardel R, Nagel M, Nu F, Lippert T, Wokaun A. Laser forward transfer using a sacrificial layer : influence of the material properties. Appl Surf Sci 2007;254:1322–6.
[76] Kattamis NT, Purnick PE, Weiss R, Arnold CB. Thick film laser induced forward transfer for deposition of thermally and mechanically sensitive materials and mechanically sensitive materials. Appl Phys Lett 2007;171120.
[77] Visser CW, Pohl R, Sun C, Römer G, Huis B. Toward 3D printing of pure metals by laser-induced forward transfer. Adv Mater 2015:4087–92. https://doi.org/10.1002/adma.201501058.
[78] Breckenfeld E, et al. Laser-induced forward transfer of silver nanopaste for microwave interconnects. Appl Surf Sci 2015;331:254–61.
[79] Colina M, Duocastella M, Fernandez-Pradas JM, Serra P, Morenza JL. Laser-induced forward transfer of liquids : study of the droplet ejection process. J Appl Phys 2007;99.

[80] Feinaeugle M, Pohl R, Bor T, Vaneker T, Römer G. Printing of complex free-standing microstructures via laser-induced forward transfer (LIFT) of pure metal thin films. Addit. Manuf. 2018;24:391–9.
[81] Biver E, Rapp L, Alloncle A, Serra P, Delaporte P. High-speed multi-jets printing using laser forward transfer : time-resolved study of the ejection dynamics. Optic Express 2014;22:1206–10.
[82] Piqué M, Zalalutdinov SA, Mathews A. Laser decal transfer of freestanding microcantilevers and microbridges. Appl Phys A Mater Sci Process 2009;97:513–9.
[83] Serra P, Duocastella M, Ferna JM, Morenza JL. Liquids microprinting through laser-induced forward transfer. Appl Surf Sci 2009;255:5342–5.
[84] Munoz-martin D, et al. Laser-induced forward transfer of high-viscosity silver pastes. Appl Surf Sci 2016;366:389–96.
[85] Young D, et al. Plume and jetting regimes in a laser based forward transfer process as observed by time-resolved optical microscopy. Mater Res Soc Symp Proc 2019;698:1–5.
[86] Matthews SA, Auyeung RCY, Kim H, Charipar NA, Pique A. High-speed video study of laser-induced forward transfer of silver nano-suspensions. J Appl Phys 2013;114:064910. https://doi.org/10.1063/1.4817494.
[87] Yamada H, Sano T, Nakayama T, Miyamoto I. Optimization of laser-induced forward transfer process of metal thin films. Appl Surf Sci 2002;198:411–5.
[88] Sano T, Yamada H, Nakayama T, Miyamoto I. Experimental investigation of laser induced forward transfer process of metal thin films. Appl Surf Sci 2002;186:221–6.
[89] Kuznetsov AI, Koch J, Chichkov BN, Zentrum L. Laser-induced backward transfer of gold nanodroplets. Optic Express 2009;17:18820–5.
[90] Kuznetsov AI, et al. Laser-induced transfer of metallic nanodroplets for plasmonics and metamaterial applications. J Opt Soc Am B 2009;26:B130.
[91] Patrascioiu A, et al. Interaction between jets during laser- induced forward transfer. Appl Phys Lett 2014;105.
[92] Auyeung RCY, Kim H, Mathews S, Piqué A. Laser forward transfer using structured light. Optic Express 2015;23:422–30.
[93] Heath DJ, Feinaeugle M, Grant-jacob JA, Mills B, Robert W. Dynamic spatial pulse shaping via a digital micromirror device for patterned laser-induced forward transfer of solid polymer films. Opt Mater Express 2015;5:4843–9.
[94] Duocastella M, Kim H, Serra P. Optimization of laser printing of nanoparticle suspensions for microelectronic applications. Appl Phys A 2012;106:471–8.
[95] Kuznetsov AI, et al. Laser fabrication of large-scale nanoparticle arrays for sensing applications. ACS Nano 2011;5:4843–9.
[96] Manogharan GP, et al. Making sense of 3-D printing: creating a map of additive manufacturing products and services. Addit. Manuf. 2014;1–4:64–76.
[97] Guo N, Leu MC. Additive manufacturing: technology, applications and research needs. Front Mech Eng 2013;8:215–43.
[98] Bourell DLD, Beaman JJ, Leu MC, Rosen DW. A brief history of additive manufacturing and the 2009 roadmap for additive manufacturing: looking back and looking ahead. US-Turkey Work 2009. https://doi.org/10.1089/3dp.2013.0002. 2005–2005.
[99] Sing SL, et al. Review of selective laser melting: materials and applications. Appl Phys Rev 2015;2. 041101.
[100] Liu R, Wang Z, Sparks T, Liou F, Newkirk J. Aerospace applications of laser additive manufacturing. Laser additive manufacturing: materials, design, technologies, and applications. Elsevier Ltd; 2016. https://doi.org/10.1016/B978-0-08-100433-3.00013-0.
[101] Wong M, Tsopanos S, Sutcliffe CJ, Owen I. Selective laser melting of heat transfer devices. Rapid Prototyp J 2007;13:291–7.
[102] Yadroitsev I, Krakhmalev P, Yadroitsava I. Selective laser melting of Ti6Al4V alloy for biomedical applications: temperature monitoring and microstructural evolution. J Alloys Compd 2014;583:404–9.
[103] Vaezi M, Seitz H, Yang S. A review on 3D micro-additive manufacturing technologies. Int J Adv Manuf Technol 2013;67:1721–54.
[104] Hirt L, Reiser A, Spolenak R, Zambelli T. Additive manufacturing of metal structures at the micrometer scale. 2017. p. 1604211.
[105] Roy NK, Foong CS, Cullinan MA. Design of a micro-scale selective laser sintering system. In: Proceedings of the 26th annual international solid freeform fabrication symposium – an additive manufacturing conference; 2016. p. 1495–508.
[106] Roy NK, Behera D, Dibua OG, Foong CS, Cullinan M. Experimental study of the subsystems in a microscale Additive manufacturing process. JOM 2018. https://doi.org/10.1007/s11837-018-3223-3.
[107] Roy NK, Foong CS, Cullinan MA. Effect of size, morphology , and synthesis method on the thermal and sintering properties of copper nanoparticles for use in microscale additive manufacturing processes. Addit. Manuf. 2018;21:17–29.
[108] Volkman SK, et al. Mechanistic studies on sintering of silver nanoparticles. 2011. https://doi.org/10.1021/cm202561u.
[109] Nanda KK, Maisels A, Kruis FE, Fissan H, Stappert S. Higher surface energy of free nanoparticles. 2003. p. 1–4. https://doi.org/10.1103/PhysRevLett.91.106102.
[110] Roy N, et al. Laser sintering of copper nanoparticles: a simplified model for fluence estimation and validation. In: ASME 2017 12th international manufacturing science and engineering conference; 2017. p. 1–7. https://doi.org/10.1115/MSEC2017-2975.
[111] Roy N, Dibua O, Foong CS, Cullinan M. Preliminary results on the fabrication of interconnect structures using microscale selective laser sintering. In: ASME 2017 international technical conference and exhibition on packaging and integration of electronic and photonic microsystems (InterPACK2017); 2017. p. 1–7. https://doi.org/10.1115/IPACK2017-74173.
[112] Lu K. Sintering of nanoceramics. Int Mater Rev 2008;53:21–39.
[113] Ze M, Shomrat N, Tsur Y. Recent advances in mechanism research and methods for electric-field-assisted sintering of ceramics, vol. 1706369; 2018. p. 1–8.
[114] Hagen D, Kovar D, Beaman JJ. Effects of electric field on selective laser sintering of yttria-stabilized zirconia ceramic powder. 2018. p. 909–13.
[115] Roy NK, Dibua OG, Cullinan MA. Effect of bed temperature on the laser energy required to sinter copper nanoparticles. Jom 2018;70:401–6.
[116] Dibua OG, Yuksel A, Roy NK, Foong CS, Cullinan M. Nanoparticle sintering Model : simulation and calibration against experimental data. ASME J. Micro-and Nano-manufacturing 2019;6.
[117] Roy NK, Behera D, Dibua OG, Foong CS, Cullinan MA. Single shot, large area metal sintering with micrometer level resolution. Optic Express 2018;26:25534.
[118] Roy NK, Behera D, Dibua O, Foong C, Cullinan MA. A novel microscale selective laser sintering (μ-SLS) process for the fabrication of microelectronic parts. Nat. Microsystems Nanoeng. 2019;5.
[119] Roy NK, et al. A comprehensive study of the sintering of copper nanoparticles using femtosecond, nanosecond, and continuous wave lasers. J Micro Nano-Manufacturing 2017;6:010903.
[120] Capodieci L. From optical proximity correction to lithography-driven physical design (1996-2006): 10 years of resolution enhancement technology and the roadmap enablers for the next decade. In: SPIE 31st international symposium on advanced lithography - optical microlithography XIX, vol. 6154; 2006. p. 615401.
[121] Theodorakos I, Zacharatos F, Geremia R, Karnakis D, Zergioti I. Selective laser sintering of Ag nanoparticles ink for applications in flexible electronics. Appl Surf Sci 2015;336:157–62.
[122] Roy NK, Cullinan MA. Fast trajectory tracking of a flexure-based, multiaxis nanopositioner with 50-mm travel. IEEE/ASME Trans. Mechatronics 2018;23:2805–13.
[123] Behera D, Roy NK, Foong CS, Cullinan M. Nanoparticle bed deposition by slot die coating for microscale selective laser sintering applications. In: Proceedings of the 29th annual international solid freeform fabrication symposium - an additive manufacturing conference; 2018. p. 2382–93.
[124] Ashkin A. Acceleration and trapping of particles by radiation pressure. Phys Rev Lett 1970;24:156–9.
[125] Ashkin A, Dziedzic JM, Yamane T. Optical trapping and manipulation of single cells using infrared laser beams. Nature 1987;330:769–71.
[126] Ashkin A, Dziedzic JM. Optical levitation in high vacuum. Appl Phys Lett 1976;28:333–5.
[127] Ashkin A. Forces of a single-beam gradient laser trap on a dielectric sphere in the ray optics regime. Biophys J 1992;61:569–82.
[128] Svoboda K, Block SM. Optical trapping of metallic Rayleigh particles. Opt Lett 1994;19:930.
[129] Chu S, Bjorkholm JE, Ashkin A, Cable A. Experimental observation of optically trapped atoms. Phys Rev Lett 1986;57:314–7.
[130] Ashkin A. Forces of a single-beam gradient laser trap on a dielectric sphere in the ray optics regime. Methods Cell Biol 1998;55:1–27.
[131] Ke PC, Gu M. Characterization of trapping force on metallic Mie particles. Appl Optic 1999;38:160.
[132] Grier DG. A revolution in optical manipulation. Nature 2003;424:810–6.
[133] Dufresne ER, Grier DG. Optical tweezer arrays and optical substrates created with diffractive optics. Rev Sci Instrum 1998;69:1974.
[134] Curtis JE, Koss BA, Grier DG. Dynamic holographic optical tweezers. Optic Commun 2002;207:169–75.
[135] Dufresne ER, Spalding GC, Dearing MT, Sheets SA, Grier DG. Computer-generated holographic optical tweezer arrays. Rev Sci Instrum 2001;72:1810.
[136] Gerchberg RW, Saxton WO. A practical algorithm for the determination of phase from image and diffraction plane pictures. Optik (Stuttg). 1972;35:237–46.
[137] Chizari S, Lim M, Shaw L, Austin S, Hopkins JB. Automated optical-tweezers assembly of engineered microgranular crystals. Small 2020;16.
[138] Grier DG, Roichman Y. Holographic optical trapping. Appl Optic 2006;45:880.
[139] Resnick A. Use of optical tweezers for colloid science. J Colloid Interface Sci 2003;262:55–9.
[140] Grier DG. Optical tweezers in colloid and interface science. Curr Opin Colloid Interface Sci 1997;2:264–70.
[141] Kampmann R, Chall AK, Kleindienst R, Sinzinger S. Optical system for trapping particles in air. Appl Optic 2014;53:777.
[142] Nieminen TA, et al. Optical tweezers computational toolbox. J. Opt. A Pure Appl. Opt. 2007;9:S196–203.
[143] Curtis JE, Grier DG. Structure of optical vortices. Phys Rev Lett 2003;90:133901.
[144] van der Horst A, van Oostrum PDJ, Moroz A, van Blaaderen A, Dogterom M. High trapping forces for high-refractive index particles trapped in dynamic arrays of counterpropagating optical tweezers. Appl Optic 2008;47:3196.
[145] Spesyvtseva SES, Dholakia K. Trapping in a material world. ACS Photonics 2016;3:719–36.
[146] Ghadiri R, Weigel T, Esen C, Ostendorf A. Microfabrication by optical tweezers. In: Pfleging W, Lu Y, Washio K, editors. Proc. Of SPIE, vol. 7921; 2011. 792102-792102–9.
[147] Jordan P, et al. Permanent 3D microstructures in a polymeric host created using holographic optical tweezers. J Mod Optic 2004;51:627–32.
[148] Shaw LA, Chizari S, Hopkins JB. Improving the throughput of automated holographic optical tweezers. Appl Optic 2018;57:6396.
[149] Chapin SC, Germain V, Dufresne ER. Automated trapping, assembly, and sorting with holographic optical tweezers. Optic Express 2006;14:13095–100.
[150] Peng T, Balijepalli A, Gupta SK, LeBrun T. Algorithms for on-line monitoring of micro spheres in an optical tweezers-based assembly cell. J Comput Inf Sci Eng 2007;7:330.

[151] Fällman E, Axner O. Influence of a glass-water interface on the on-axis trapping of micrometer-sized spherical objects by optical tweezers. Appl Optic 2003;42:3915–26.
[152] Won J, et al. Photothermal fixation of laser-trapped polymer microparticles on polymer substrates. Appl Phys Lett 1999;75:1506–8.
[153] Shaw LA, et al. Holographic optical assembly and photopolymerized joining of planar microspheres. Opt Lett 2016;41.
[154] Misawa H, Sasaki K, Koshioka M, Kitamura N, Masuhara H. Laser manipulation and assembling of polymer latex particles in solution. Macromolecules 1993;26:282–6.
[155] Ghadiri R, Weigel T, Esen C, Ostendorf A. Microassembly of complex and three-dimensional microstructures using holographic optical tweezers. J Micromech Microeng 2012;22:065016.
[156] Rodrigo PJ, et al. Optical microassembly platform for constructing reconfigurable microenvironments for biomedical studies. Optic Express 2009;17:6578.
[157] Rodrigo PJ, et al. 2D optical manipulation and assembly of shape-complementary planar microstructures. Optic Express 2007;15:9009.
[158] Köhler J, Ksouri SI, Esen C, Ostendorf A. Optical screw-wrench for microassembly. Microsystems Nanoeng 2017;3:16083.
[159] Köhler J, et al. Optical assembly of microsnap-fits fabricated by two-photon polymerization. Opt Eng 2017;56:1.
[160] Dawood F, Qin S, Li L, Lin EY, Fourkas JT. Simultaneous microscale optical manipulation, fabrication and immobilisation in aqueous media. Ch emical Sci 2012;3:2449.
[161] Chizari S, Shaw LA, Hopkins JB. Simultaneous printing and deformation of microsystems via two-photon lithography and holographic optical tweezers. Mater. Horizons 2019;6:350–5.
[162] Tanaka T, Ishikawa A, Kawata S. Two-photon-induced reduction of metal ions for fabricating three-dimensional electrically conductive metallic microstructure. Appl Phys Lett 2006;88:081107.
[163] Brigo L, et al. 3D nanofabrication of SiOC ceramic structures. Adv Sci 2018;5:1800937.
[164] Pham TA, et al. Three-dimensional SiCN ceramic microstructures via nano-stereolithography of inorganic polymer photoresists. Adv Funct Mater 2006;16:1235–41.
[165] Zhang X, Jiang X, Sun C. Micro-stereolithography of polymeric and ceramic microstructures. Sensors Actuators A Phys 1999;77:149–56.
[166] Askari M. Metamaterial fabrication using combined multiphoton polymerization and optical trapping. University of Nottingham; 2017.
[167] Shaw LA, Chizari S, Dotson M, Song Y, Hopkins JB. Compliant rolling-contact architected materials for shape reconfigurability. Nat Commun 2018;9:4594. https://doi.org/10.1038/s41467-018-07073-5.
[168] Roichman Y, Grier DG. Holographic assembly of quasicrystalline photonic heterostructures. Optic Express 2005;13:5434.
[169] Shaw LA, Spadaccini CM, Hopkins JB. Scanning holographic optical tweezers. Opt Lett 2017;42:2862.
[170] Deng Y, Bechhoefer J, Forde NR. Brownian motion in a modulated optical trap. J. Opt. A Pure Appl. Opt. 2007;9.
[171] Ingle N, Mohanty SK. Development of a two-photon polymerization and optical tweezers microscope for fabrication and manipulation of microstructures. Microscope 2011;7950:1–7.
[172] Ghadiri R, Surbek M, Esen C, Ostendorf A. Optically based manufacturing with polymer particles. Phys. Procedia 2010;5:47–51.
[173] Shen Z, Su L. Plasmonic trapping and tuning of a gold nanoparticle dimer. Optic Express 2016;24:4801.
[174] Bradac C. Nanoscale optical trapping: a review. Adv. Opt. Mater. 2018;6:1800005.
[175] Fan H, et al. Confined whispering-gallery mode in silica double-toroid microcavities for optical sensing and trapping. Optic Commun 2019;434:97–103.
[176] Ilic O, Atwater HA. Self-stabilizing photonic levitation and propulsion of nanostructured macroscopic objects. Nat Photon 2019;13:289–95.
[177] Hell SW, Wichmann J. Breaking the diffraction resolution limit by stimulated emission: stimulated-emission-depletion fluorescence microscopy. Opt Lett 1994;19:780.
[178] Chong C, Porter MA, Kevrekidis PG, Daraio C. Nonlinear coherent structures in granular crystals. 2016. https://doi.org/10.1088/1361-648X/aa7672.
[179] Lash MH, Fedorchak MV, McCarthy JJ, Little SR. Scaling up self-assembly: bottom-up approaches to macroscopic particle organization. Soft Matter 2015;11:5597–609.
[180] Song Y, Panas RM, Hopkins JB. A review of micromirror arrays. Precis Eng 2018;51:729–61.
[181] Fraternali F, Porter MA, Daraio C. Optimal design of composite granular protectors. Mech Adv Mater Struct 2009;17:1–19.
[182] Mizeikis V, Juodkazis S, Marcinkevičius A, Matsuo S, Misawa H. Tailoring and characterization of photonic crystals. J Photochem Photobiol C Photochem Rev 2001;2:35–69.
[183] Donahue CM, Anzel PWJ, Bonanomi L, Keller TA, Daraio C. Experimental realization of a nonlinear acoustic lens with a tunable focus. Appl Phys Lett 2014;104:014103.